Response to the reviews

In bolt: text added
Referee 1

Overall this is an interesting paper, but i think it requires some more scientific thought and the quality of the analysis and figures require improvement. As is the paper reads like a conference paper, not a journal paper. In general it is an interesting idea, but the tests are limited to three sites with dramatically different settings. This limits the authors ability to quantify the method, they should have focused on a slope type (close and rock, or far and soil) and tested three or four of that type. This would have led to a more robust analysis and conclusion. As it stands the authors state it works in some places better than others based on picture quality, lightening, etc. These are not geotechnical qualities, which should have been the focus. If the focus was on image quality, NHESS is the wrong journal for submission. I encourage the authors to dive deeper into their work and test many more sites and resubmit. Some specific comments: Stating LiDAR is expensive and demanding from a logistics point of view is irrelevant, especially when referencing a paper from 2014, that was likely written in 2012 or 2013. Modern applications of lidar are neither of those. Avoid general language with little meaning like "reasonably good" You state in Section 4 VisualSFM gave the 'best results' – this is arbitrary, you need numbers to back this up. What metric are you using to define 'best'? Section 4.1: Standard deviation of the error below 20 cm – what error are you assessing? 3D vector, Z, or XY? Your volume estimates do not have ranges, yet your point cloud has alignment errors. You should report volumes with +/- amounts. Again, 'reasonably good' should not be used in a scientific paper. Same for 'We hardly perceive' 'Same strong radial' ? In your conclusions you state the method is useful to 'quantify slope movements and displacements' yet you did not show this anywhere in your paper. You showed the ability to measure failed volumes, not displacements. This is a misleading conclusion. On your change mapping images the colours below the limit of detectable change should be coloured grey. All figures need a scale bar. Figure caption 5 is too long. The min and max difference calculated in Table 1 adds no value, those points are likely outliers.

Comment: In general it is an interesting idea, but the tests are limited to three sites with dramatically different settings. This limits the authors ability to quantify the method, they should have focused on a slope type (close and rock, or far and soil) and tested three or four of that type.
Answer: *The idea behind the three different sites is to demonstrate the capacity of the method to work on different topographic areas with different slope types with different distances image point of view – site. The first site (Monaco) shows the modelling of an anthropic slope with a wall collapse. The danger of wall collapse on a transportation track can be found everywhere around the world. We find that this case study is pertinent because it is representative of a real danger for transportation networks. Site 2*

(Séchilienne) shows the capacity of the proposed method to model a large landslide away from the road. With 6 different time steps, results shows a slope evolution over the years which corresponds to the surface changes measured with LiDAR scans. The accuracy is obviously lower as the LiDAR accuracy, but it allows to observe the main surface change. The third site (Arly) focus on a steep slope threatening a road tunnel entry. A rockfall occurred already on this area and protective measures have been built. This site shows the limit of the method in the vertical axis because some images were taken close to the cliff which is much higher than the Monaco wall. We believe that the three sites on different slopes and different settings shows the capacity and limits of the method which can be deployed on several topographic situations.

Comment: As it stands the authors state it works in some places better than others based on picture quality, lightening, etc. These are not geotechnical qualities, which should have been the focus. If the focus was on image quality, NHESS is the wrong journal for submission. I encourage the authors to dive deeper into their work and test many more sites and resubmit.
Answer: *The manuscript presents a uncommon free method that obtain 3D point cloud of a slope without field visit. The focus is clearly not on image quality, but image quality must be mentioned as it is an important condition to obtain results. This is why those "no geotechnical qualities" are mentioned. With the manuscript improvement (see below), it focuses now more on the method (with an added flowchart) and its results.*

Comment: Some specific comments: Stating LiDAR is expensive and demanding from a logistics point of view is irrelevant, especially when referencing a paper from 2014, that was likely written in 2012 or 2013. Modern applications of lidar are neither of those
Answer: *Although LiDAR references are indeed not so actual, we still maintain that LiDAR, compared to the proposed method (free, any field work), is still more expensive and more demanding from a logistics point of view (except handle LiDAR like GeoSlam for the logistic point of view). Scanning cliffs of the case studies demand few hours of field work (as we made on site 2 and site 3).*

Comment: Avoid general language with little meaning like "reasonably good" You state in Section 4 VisualSFM gave the 'best results' – this is arbitrary, you need numbers to back this up. What metric are you using to define 'best'?
Answer: *We totally agree with this remark. We try to define our magnitude order assessment with values or examples. We have for example now: "***This accuracy allows to detect object of tens cetimeters size***" still "reasonably good results". "Best results" terms have been deleted.*

Comment: Section 4.1: **Standard deviation** of the error below 20 cm – what error are you assessing? 3D vector, Z, or XY? Your volume estimates do not have ranges, yet your point cloud has alignment errors.

Answer: *"Error" is a wrong term. It is a distance between a mesh and a point cloud. The computed distance is a 3D vector from the mesh triangle to the cloud point. The sentence is now:* "**The computed shortest distance, in signed values, between the mesh and the point cloud is a 3D vector from the mesh triangle to the 3D point.**" *(Page 4, line 29)*

https://www.geometrictools.com/Documentation/DistancePoint3Triangle3.pdf

https://tel.archives-ouvertes.fr/file/index/docid/500182/filename/manuscrit_19052006_electronic.pdf

(Page 36, Section 2.2.1, Figure 2.1 of the linked document)

Comment: In your conclusions you state the method is useful to 'quantify slope movements and displacements' yet you did not show this anywhere in your paper. You showed the ability to measure failed volumes, not displacements. This is a misleading conclusion.

Answer: *Right, "displacement" is term a little bit too optimistic. It is possible to detect displacement in specific cases (displacement of few meters between the image sets, 3D point cloud with a accuracy of few decimetres, etc.) but we have replaced the term "displacement" with "surface changes". Surface change on site 1 is the wall collapse, on site 2 it is the rockfall deposit and the rockfall scare, on site 3 there is no surface change because the landslide is located on a cliff part not visible with the GSV images.*

Comment: On your change mapping images the colours below the limit of detectable change should be coloured grey. All figures need a scale bar. Figure caption 5 is too long.

Answer: *All figures have a scale bar. Figure 5 is cut into 2 different figures with 2 captions.*

Comment: The min and max difference calculated in Table 1 adds no value, those points are likely outliers.

Answer: *Right, the min and max differences were deleted because their contribution was not very interesting for this manuscript. Point density of the 3D point cloud replaces those deleted values in the Table 1.*

Referee 2

This is a very interesting paper with very useful and innovative ideas and I believe that research towards this direction is promising. However, reading the manuscript I missed a strong and solid part on technical specifications for the methodology that is used and for the quantitative analysis of the results, which is the core and the added value of this work. In that sense, I suggest to the authors, to enrich and support the description of the methodology, providing detailed information on the processes followed and to present a more thorough and detailed analysis of their results, in quantitative terms.

<u>Answer:</u> "Methodology" (#3) and "Results and discussion" (#4) sections have been significantly rewritten. Table 2 has been added, as Figures 3, 8 and 9.

Page 3: Lines 19-20

If these parameters are not known beforehand, three pictures is the minimum requirement (Westoby 2012), **and** about six pictures is preferred.

<u>Answer:</u> "And" added.

Page 4: Lines 16-17

We used two image sets from for the first study site, ~~height~~ **eight** images sets for the second study site and four image sets for the third study site, with dates ranging from May 2008 up to December 2016, as described in table 1.

<u>Answer:</u> "Height" replaced by "eight".

Page 4: Lines 26-29

To perform temporal comparisons on each site, images were taken at the different dates proposed by GSV. We used the SfM-MVS programs VisualSFM (Wu 2011) and Agisoft PhotoScan (Agisoft 2015) for dense point cloud reconstruction and CloudCompare (Girardeau-Montaut 2011) for point cloud visualization and comparison. Comparison between two point clouds was made using point-to-mesh strategy.

<u>Question:</u> It would be interesting to explain here, how the scaling and georeferencing was done, if you used control points and how many of them.

<u>Answer:</u> Sentence replaced by: "To perform temporal comparisons on each site, images were taken at the different dates proposed by GSV **with pre- and post-event images sets**. We used the SfM-MVS program VisualSFM (Wu 2011) **for dense point cloud reconstruction for the print screens images from Google Maps** and we used CloudCompare (Girardeau-Montaut 2011) software for point cloud visualization and comparison. Comparison between two point clouds was made using point-to-mesh strategy."

Further, sentence added: "**The rough scaling and georeferencing of the obtained 3D point clouds were been made without ground control points but only with coordinates of few points extracted from Google Maps or French geoportal (Géoportail, 2016).**"

Page 5: Line 1

from print screens

Question: what is the resolution of the images print screen? could you please provide some more technical information on the process and the result of the print screen? Are there certain specifications in order to achieve the result that you mention here?

Answer: Sentence replaced by: "Beside the images taken from print screens as described above, we also obtained GSV images **(4800 x 3500 pixels, 16.8 Mpx)** from Google Earth Pro on sites 2 and 3 with the "save image" function." *for resolution information.*

Further, sentence modified: "In addition, GoPro Hero4+ images from a moving vehicle on the road were taken by the authors on site 2, as well a series of images captured using a GoPro Hero5 Black camera standing on site 3 **(image resolution of 4000 x 3000 pixels, 12 Mpx)**."

Following sentence modified and replaced by (about the process): "**This second way to get GSV allows to obtain images with a higher resolution as print screen images**. Unfortunately, there is no timeline function in this program and it is only possible to save Google Earth Pro images from the last picture acquisition, **i.e. generally post-event images. GSV images from Google Earth Pro were processed with the Agisoft PhotoScan (Agisoft 2015) software for dense point cloud reconstruction. The reason why we chose Visual SFM software to process GSV print screens images from Google Maps is because the processing of those print screens with Agisoft PhotoScan software is not possible while results of GSV images processing from Google Earth Pro is clearly better with Agisoft. The flowchart of SfM-MVS with GSV images combines also two image types from two different sources (print screens and saved images) processed into two softwares (Figure 3).**"

Figure 3 added (process flowchart): "**Flowchart of the SfM-MVS processing with GSV images on an area with the"back in time" function available. Pre-event images are print screens of GSV in Google Maps. Those GSV images are displayed using the "back in time" function in GSV and are processed in Visual SFM software. Post-event images arise either from print screens of GSV in Google Maps using or not the "back in time" function or from GSV images saved in Google Earth Pro. In this last case, the last available proposed GSV images have a greater resolution as the print screens and can be processed in the Agisoft PhotoScan software.** (*Figure 3 caption).*

Page 5: Line 12

This information was used for quality assessment purposes.

Question: It would be useful here, to get some information on the resolution of the images in each case.

Answer: Image resolution is now given (please see previous question).

Page 5: Lines 9-17

Different results are obtained as a function on the software used for SfM-MVS processing. VisualSFM gave the best results with print screens from GSV while Agisoft PhotoScan could not align any GSV images from Google Maps print screens despite adding a series of control points measured with Google Earth Pro. However, Agisoft PhotosScan provided better results with images from Google Earth Pro than VisualSFM.

Question: Is it the same for all the case studies? Any possible interpretation?

Answer: Sentence modified: Different results are obtained as a function on the software used for SfM-MVS processing**. For all case studies**, VisualSFM gave the best results with print screens from GSV while Agisoft PhotoScan could not align any GSV images from Google Maps print screens despite adding a series of control points measured with Google Earth Pro. **Resolution of print screens images seem the be insufficient to be processed with Agisoft PhotoScan**. However, Agisoft PhotosScan provided better results with images from Google Earth Pro than VisualSFM.

Page 5: Line 23

The alignment of both point clouds was done on a stable part of the cliff, with a standard deviation of the error below 20 cm (Figure 3C).

Question: What software has been used to htis end?

Answer: Paragraph modified: "It was possible on "Basse Corniche" site to estimate the fallen volume by scaling and comparing the 2008 (**Figure 4A**) and 2010 (**Figure 4B**) point clouds. **The 2008 3D point cloud is composed of 150'000 points with an average density of 290 points per square meter and the 2014 3D point cloud is composed of 182'000 points with an average density of 640 points per square meter (Table 1**). VisualSFM software could align the images and make 3D models before and after the wall collapse. It was possible to roughly scale **and georeference** the scene with the road width **and few point coordinates** measured on Google Earth Pro and on the French geoportal (Géoportail, 2016). After aligning the two 3D point clouds, meshes were built to compute the collapsed volume. The **point to mesh** alignment **in CloudCompare software** of both point clouds was done on a **small** stable part of the cliff with a standard deviation of the error below 10 cm (Figure 4C) **and on the entire cliff beside the vegetation with a standard deviation of about 25 cm (Figure 4E).**"

Page 6: Lines 7-9

The number of 3D points on the landslide area varies from 9’500 to 25’000 points for a processing with VisualSFM, while 236’000 3D points were generated when using Agisoft PhotoScan.

<u>Question:</u> What is the distance between points? Is the distance variating significantly as the distance from the camera increases?

<u>Answer:</u> in the Discussion (4.4), paragraph and figure (Figure 7) added: “**The point density was evaluated according to the distance between the image point of view and the subject and the image types and processing softwares. The obtained results and the derived trends indicate that the use of GSV images from Google Earth Pro with Visual SFM software increases of factor two the point density compared as the processing of GSV print screens with Visual SFM. The processing of GSV images from Google Earth Pro with Agisoft PhotoScan software increases of factor ten the point density compared as the processing of GSV print screens with Visual SFM (trend lines in Figure 7). Concerning the distance image point of view - area, the expected point density of the 3D point cloud from GSV print screens processed in Visual SFM software of a subject located few meters nears to the camera point of view (“Monaco” dots on Figure 7) is about 300 points/m2, about 50 points/m2 for an area located at about 100 m (“Arly” dots on Figure 7) and about 0.5 point/m2 for an area located at about 700 m (“Séchilienne” dots on Figure 7).**”

Figure 7 caption: “**Correlation between distance camera - case studies and the expected density of points from the three case studies. The red colour dots are results of the three case studies point clouds obtained from Google Street View (GSV) print screens (PS) in Google Maps (GM) processed with Visual SFM software. The red colour dash line represents their trend line based on the three case studies. The orange colour dot is the result of the Séchilienne point cloud obtained from GSV images saved in Google Earth Pro (GEP) processed with Visual SFM software. The orange colour dash line is its estimated trend line only based on the Séchilienne point cloud (point density multiplied by three compared to the red colour trend line). The green colour dots are results of the Séchilienne and Arly point clouds obtained from GSV images saved in (GEP) processed with Agisoft PhotoScan software. The green colour dash line is their estimated trend line based only on the Arly and Séchilienne point clouds (point density multiplied by eleven compared to the red colour trend line). By way of comparison, the blue colour dots represent the result of the Séchilienne and Arly point clouds obtained with GoPro action camera images taken on the field and processed with Agisoft PhotoScan software.**”

Page 6: Line 12

(distance point to mesh in absolute values)

<u>Question:</u> the absolute value would be 2.1 and not -2.1.

<u>Answer:</u> Paragraph modified. Those values were deleted.

Page 6: Line 23

less accurate when using SfM-MVS processing

<u>Question:</u> *Please explain*

<u>Answer:</u> *I think that it is now understandable with the different added text in the manuscript that low resolution print screens with Visual SFM software provide less accurate results as images saved from Google Earth Pro an processed in Agisoft PhotoScan software.*

Sentence modified: "Results were less accurate when using SfM-MVS processing with VisualSFM and lower resolution print screen images from Google Maps **probably due to the too low image resolution of those print screens**."

Page 7: Lines 16-17

the GNSS integrated in the camera;

<u>Question:</u> *What about its scaling and orientation?*

<u>Answer:</u> *Sentence modified:"* The 3D point cloud from the GoPro Hero5 Black images has been roughly georeferenced, **scaled and oriented** thanks to the GNSS **chip** integrated in the camera **and has been controlled and refined with point coordinate extracted from Google Maps and the French geoportal**."

Page 7: Line 20

gives the least accurate results (Figure 5A).

<u>Question:</u> *please provide some quantitative information on the accuracy (level of error, point cloud density). How are the errors distributed all the point cloud, with respect to the distance from the photo camera?*

<u>Answer:</u> *it converges to the question "Page 6: Lines 7-9". In all paragraphs of section 4 "Results and discussion", there is now more information about the clouds comparison.*

Page 9: Line 12-13

According to the results, small-scale landslides and rockfalls (<1 m3) can be detected when the slope or the cliff is close to the road (0-10 m), as it was shown on site 1.

<u>Question:</u> *Are there areas where this small changes correspond to errors an although they have been detected, they are not realistic? Is their proportion important? Could you please comment on that?*

<u>Answer:</u> *Sentence further added:* "**On such sites, small changes (<1 m3) can correspond to as well as realistic rockfalls as errors resulting of from processing like on the toe of the almost all Séchilienne landslide 3D point clouds (Figure 5 A2-H2).**"

Page 9: Lines 18-19

This is attributable to the occurrence of slope movements generating material increase or decrease and thereby, increasing standard deviations of the error.

Question: *In the case of low density of the point cloud (of some meters of example), the roughness of the terrain in case study 2, due to the different sized of the deposited blocks plays an important role when aligning the point clouds and calculating the errors. How has this been taken into consideration, where the point cloud density is low?*

Answer: *Sentences added: "***It can also be due to a bad 3D point cloud alignment. Indeed, the cloud alignments is not always easy on some point clouds because of low point density, because of voids in the point clouds (like in the landslide toe in Figure 5 F2) and because of the roughness of the terrain due to the different sized of the deposited blocks. In such difficult alignment cases, it was tried to align the point clouds on parts where the point cloud quality was the best to make an alignment and where the parts were stables.**"

Page 17: Lines 1-5

Figure 4: Results at site 2 "Séchilienne". Eight points clouds from different images sets taken at six different time with three different image sources and processed with two different programs. Figures A1-H1: Meshs resulting from the respective point clouds. Figures A2-H2: point clouds comparison with a 50 cm LiDAR DEM from 2010 (red colour points is material increase; blue colour points are material decrease from the 2010 LiDAR cloud). The information on the pictures source and date and on the program used is given in Table 1.

Question: *I think it would help to use the same colour scale for the easier comparison of the displacements at different point clouds.*

Answer: *All scales are now similar (-5 to +5 m).*

Using street view imagery for 3D survey of rock slope failures

J., Voumard[1], A., Abellan[1,2], P., Nicolet[1,3], M.-A. Chanut[4], M.-H., Derron[1], M., Jaboyedoff[1]

[1] Risk analysis group, Institute of Earth Sciences, FGSE, University of Lausanne, Switzerland
[2] Scott Polar Research Institute, Department of Geography, University of Cambridge, United Kingdom
[3] Geohazard and Earth Observation team, Geological Survey of Norway (NGU), Norway
[4] Groupe Risque Rocheux et Mouvements de Sols (RRMS), Cerema Centre-Est, France

Formatte

Formatte

Abstract

We discuss here ~~the~~different challenges and limitations on surveying rock slope failures using 3D reconstruction from ~~images~~image sets acquired from Street View Imagery (SVI~~) and processed with modern photogrammetric workflows.~~). We show how ~~the "back in time" function~~rock slope surveying can be ~~used for a 3D reconstruction of~~performed using two or more image sets using online imagery with photographs from the same site but acquired at different instants~~ of time, allowing for rock slope surveying.~~. Three sites in the French alps were selected~~: (a~~ as pilot study areas: (1) a cliff beside a road where a protective wall collapsed consisting ~~on~~of two images sets (60 and 50 images ~~on~~in each set) captured ~~on~~within a six years ~~timeframe; (b~~time-frame; (2) a large-scale active landslide located on a slope at 250 m from the road, using seven images sets (50 to 80 images per set) from 5 different time periods with three images sets for one period; (~~c~~3) a cliff over a tunnel which has collapsed, using two ~~images~~image sets ~~on~~captured in a four years time-frame. The analysis ~~includes~~include the use of different ~~commercially available~~ Structure for Motion (SfM) programs and the comparison between the so-extracted photogrammetric point clouds and a LiDAR derived mesh that was used as a ground truth. ~~As a result,~~Results show that both landslide deformation ~~together with~~and estimation of fallen volumes were clearly identified in the different point clouds. Results are site and software-dependent, as a function of the image set and number of images, with model accuracies ranging between 0.2 and 3.8 m in the best and worst scenario, respectively. ~~Despite~~Although some ~~clear~~ limitations ~~and challenges~~derived from the generation of 3D models from SVI were observed, this ~~manuscript demonstrates that this original~~ approach ~~might~~ allow obtaining preliminary 3D models of an area without on-field images~~. Furthermore,~~, allowing extracting the pre-failure topography ~~can be obtained for sites where it~~that would not be available otherwise.

Keywords

Street ~~view imagery,~~View Imagery (SVI), Structure from Motion~~,~~ (SfM), photogrammetry, 3D point cloud, natural hazard, landslide, rockfall.

1 Introduction

3D remote sensing techniques are becoming widely used for geohazard investigations due to their ability to represent the geometry of natural hazards (mass movements, lava flows, debris flows, etc.) and its evolution over time by comparing 3D point clouds acquired at different time steps. For example, 3D remote sensing techniques are helping to better quantify key aspects of rock slope evolution, including the accurate quantification of rockfall rates and the deformation of rock slopes before failure using both LiDAR (Rosser et al., 2005; Oppikofer et al, 2009; Royan et al., 2013; Kromer et al., 2015; Fey and Wichmann., 2016) and photogrammetrically derived point clouds (Walstra et al., 2007; Lucieer et al., 2013, Stumpf et al., 2015; Fernandes et al., 2016; Guerin et al., ~~2016~~2017; Ruggles et al., 2016).

Airborne and terrestrial laser scanner (ALS and TLS, respectively) are commonly used techniques to obtain 3D digital terrain models (Abellan et al., 2014). ~~.~~Despite their very high accuracy and resolution, these technologies are ~~expensive~~costly and often demanding from a logistic point of view~~ (Abellan et al., ~~. Alternatively,~~2014). Another way to obtain point clouds without these inconveniences is photogrammetry, in particular the~~ Structure from Motion (SfM) photogrammetry combined with multiview-stereo (MVS) ~~that~~ allow ~~generating reasonably good 3D point clouds~~ using end-user digital cameras to generate 3D point clouds with a decimetre level accuracy in a cost-effective way in order (Westoby et al., 2012; Carrivick et al., 2016).

Whereas most of the studies in SfM literature utilise pictures that were ~~directly~~ captured on~~-site,~~ purpose (Eltner et al., 2016), the potential of using internet-retrieved pictures ~~has~~for 3D reconstruction has not been fully discussed before (e.g. Snavely et al., 2008; Guerin et al., 2017). One of the large sources of pictures on-line is the Street View Imagery (SVI) services, which offer 360 degrees panoramas from many roads, streets and other places around the world (Anguelov et al, 2013). It allows to remotely observe areas ~~at a very reduced cost and~~ without physically accessing them~~. SVI is thus an interesting visual information source~~ and so in a cost-effective way, with applications in navigation, tourism, building texturing, image localization, point clouds georegistration and motion-from-structure-from-motion (Zamir et al. 2010; Anguelov et al, 2010; Klingner et al, 2013; Wang, 2013; Lichtenauer et al., 2015).

The aim of present work is to ascertain ~~whether~~up to which extent 3D models ~~be~~ derived from SVI~~ using photogrammetric workflows~~ can be used to detect geomorphic changes on rock slopes.

1.1 Street View Imagery

The most common SVI service is the well-known Google Street View (GSV) (Google Street View, 2017) that is available from Google Maps (Google Maps, 2017) or Google Earth Pro

(Google Earth Pro, 2013). We used both GSV as SVI service in this study. Alternatives include ~~Streetside~~StreetSide by Microsoft (~~Streetside~~StreetSide, 2017) and other national services like Tencent Maps in China (Tencent Maps, 2017). SVI was firstly deployed in urban areas to offer a virtual navigation into the streets. More recently, non-urban zones can also be accessed, and ~~will be~~were used for the analysis of rock slope failures in this manuscript.

~~Firstly~~GSV was firstly used in May 2007 for capturing pictures in streets of the main cities in USA~~, GSV~~ and it has been deployed worldwide over the forthcoming years, including also rural areas. GSV images are collected with a panoramic camera system mounted on different types of vehicles (e.g. a car, train, bike, snowmobile, etc.) or carried into a backpack (Anguelov et al, 2010~~) (Figure 1~~).

The GSV first generation camera system was composed of eight wide-angle lenses and it is currently composed of fifteen CMOS sensors 5Mpx each (Anguelov et al, 2010). The fifteen raw images, which are not publicly available, are processed by Google to make a panorama view containing an a priori unknown image deformation~~.~~ (Figure 1). A GSV panorama is normally taken at an interval of around ten meters along a linear infrastructure (road, train~~,~~ or path).

GSV proposes a *back-in-time function* on a certain number of locations since April 2014. ~~Historical~~In addition, other historical GSV images are available from 2007 for selected areas only. The number of available image sets greatly varies ~~a lot because it depends on the number of acquisitions made by Google. While~~at different locations: while some places have several sets, many other locations have only one image set~~, some places have several sets. This~~. Back in time function is especially useful for natural hazards because it is possible to compare pre- and post-events images.

The GSV process can be explained in four steps (Anguelov et al, 2010; Google Street View, 2017): 1) Pictures acquisition in the field; 2) Image alignment: preliminary coordinates are given for each picture, extracted from sensors on the Google car that measure GNNS coordinates, speed and azimuth of the car, helping to precisely reconstruct the vehicle path. Pictures can also be tilted and realigned as needed; 3) Creation of 360° panoramas by stitching overlapping pictures. Google applies a series of processing algorithms to each picture to attenuate delimitations between each picture and to obtain smooth pictures transitions; 4) Panoramas draping on 3D models: the three LiDAR mounted on the Google car help to build 3D models of the scenes. 360° panoramas are draped on those 3D models to give a panorama view close to the reality. Each picture of the panorama has its own internal deformation, and the application of the processing chain described above makes inconstant deformation in the 360° panorama; in addition, the end-user does not have any information or control on it.

1.2 SfM-MVS

Structure for Motion (SfM) with Multi-View Stereo (MVS) dense reconstruction is a ~~low-~~cost-effective photogrammetric method to obtain a 3D point cloud of terrain using a series of overlapping images (Luhmann et al., 2014). The prerequisites are that: (1) the studied object is photographed from different points of view, and (2) each element of the object must be captured from a minimum of two pictures assuming that the lens deformation parameters are known in advance (Snavely 2008; Lucieer et al. 2013). If these parameters are not known beforehand, three pictures is the minimum requirement (Westoby 2012), and about six pictures is preferred. The particularity of SfM-MVS is that prior knowledge of both intrinsic camera parameters (principal point, principal distance and lens distortion) and extrinsic camera parameters (orientation and position of the camera centre (Luhmann et al., 2014)) is not needed.

The workflow of SfM-MVS normally includes the following steps: 1) Feature detection and matching (Lowe, 1999); 2) Bundle adjustment (Snavely et al., 2006; Favalli et al., 2011; Turner et al., 2012; Lucieer et al., 2013); 3) Dense 3D point cloud generation (Furukawa et al., 2010; Furukawa & Ponce, 2010; James & Robson, 2012); and 4) Surface reconstruction and visualization (James & Robson, 2012).

2 Study areas and available data

We selected three study areas in France to generate point clouds from GSV images. This country was chosen because GSV cover the majority of the roads and because the timeline function works in most of the areas covered by GSV, meaning that several periods of acquisition are available. Moreover, landslide events occur regularly on French alpine roads. The aerial view of the three areas is shown in Figure 2A and examples of corresponding GSV images in Figure~~.~~ 2B and 2C.

The first case study (“Basse corniche” site) is a 20 m high cliff beside a main road in Roquebrune – Cap Martin connecting the town of Menton to the Principality of Monaco, in South-Eastern France. A wall built to consolidate the cliff collapsed after an extreme rainfall event in January 2014, blocking the road (Nice-Matin, 2014). Two 3D models were built with

60 GSV images taken in 2008 before the wall collapse, and 50 GSV images taken in 2014 after the event.

The second case studies is Séchilienne landslide, located 15 km South East of Grenoble (Isère department, France). The active area is threatening the departmental road RD 1091 connecting the towns of Grenoble and Briançon as well as a set of ski resorts such as L'Alpe d'Huez and Les Deux Alpes to the plain. This landslide is about 800 m long by 500 m high and it has been active during more than thirty years (Le Roux et al. 2009; Durville et al. 2011; Dubois et al. 2014). The shortest distance between the landslide foot and the former road was 250 m~~.~~ and the longest distance between the landslide head and the road is 1 km. A new road, located higher in the opposite slope, has been opened since July 2016. Different SfM-MVS processing were tested using from 50 up to 80 GSV images, at six different times from April 2010 to June 2015.

The third case study is located in "Arly gorges", between Ugine and Megève on the path Alberville – Chamonix-Mont-Blanc. A rockfall of about 8'000 m^3 affected the road at the entry of a tunnel on January 2014 (France 3, 2014). Different sets of images ranging from 60 to 110 GSV images were processed in order to obtain three 3D models of the road, the tunnel entry and the cliff above the tunnel.

We used two image sets from for the first study site, ~~height images~~eight image sets for the second study site and four image sets for the third study site, with dates ranging from May 2008 up to December 2016, as described in ~~table~~Table 1.

3 Methodology

First step to make SfM-MVS with SVI is to ~~get~~obtain images from a SVI service. GSV has been used in this study (~~Figure1~~Figure 1). Given that original images of the Google cameras are not available, one of the ~~only way~~two ways to get images from GSV is to manually extract them from the GSV panoramas. We took print screens (1920 x 1200 pixels, 2.3 Mpx) of GSV panoramas of the studied areas at each acquisition step~~ (~~, separated by about ten meters~~). We took several~~, from Google Maps. Several images were taken from the same point of view with different pan and tilt angles (Figure 1C) when the studied object was too close to the road. In such cases, it was impossible to have the entire area in one image because the image is not wide enough to capture the entire studied area (for example a 10 m high cliff along road). When the studied area was far away from the road, we took print screens of zoomed sections of the panorama.

To perform temporal comparisons on each site, images were taken at the different dates proposed by GSV~~.~~ with pre- and post-event images sets. We used the SfM-MVS ~~programs~~program VisualSFM (Wu 2011) ~~and Agisoft PhotoScan (Agisoft 2015)~~ for dense point cloud reconstruction for the print screens images from Google Maps and we used CloudCompare (Girardeau-Montaut 2011) for point cloud visualization and comparison. Comparison between two point clouds was made using point-to-mesh strategy. ~~A~~ To this end, a mesh ~~of one~~was generated from the reference point cloud (~~whether~~ the point cloud with the oldest images for ~~the~~ site 1 or the LiDAR scans for ~~the~~ sites 2 and 3) ~~is compared with~~and then the other point cloud was compared to ~~obtain the~~this reference mesh. The computed shortest distance ~~of each point of~~, a signed value, between the mesh and the point cloud is the length of the 3D vector from the mesh triangle to the ~~mesh~~3D point. Thus, average distances and standard deviations for each comparison of point clouds have been computed. Point density of point clouds was obtained using the “point density” function in ~~absolute values~~CloudCompare with the “surface density” option.

Beside the images taken from print screens as described above, we also obtained GSV images (4800 x 3500 pixels, 16.8 Mpx) from Google Earth Pro on sites 2 and 3 with the “save image” function. This second way to get GSV allows to get images with a higher resolution than print screen images. Unfortunately, there is no timeline (or “back in time”) function in ~~this program and~~ Google Earth Pro; it is only possible to save ~~Google Earth Pro~~ images from the last picture acquisition~~.~~, i.e. generally post-event images. GSV images from Google Earth Pro were processed with the Agisoft PhotoScan software (Agisoft 2015) for dense point cloud reconstruction, which provides much better results than VisualSFM. GSV images from Google Map were processed with VisualSFM because Agisoft was not able to process those print screens. The flowchart of Figure 3 shows the processing applied to both types of images (print screens and saved images).

A rough scaling and georeferencing of the 3D point clouds was made without ground control points, only with coordinates of few points extracted from Google Maps or from the French geoportal (Géoportail, 2016).

It is important to mention here that a series of issues are expected when attempting to use SVI for 3D model reconstruction with SfM-MVS. Indeed, GSV images are constructed as 360° panoramas from a series of pictures, so the internal deformation of the original image is not fully retained on the panoramas. In other words, the deformation of a cropped section of the panorama will be a main function not only of the internal deformation of the camera and lens but to the panorama reconstruction process; ~~This~~this circumstance will significantly influence the bundle adjustment process and so to the 3D reconstruction.

In addition, GoPro Hero4+ images from a moving vehicle on the road were taken by the authors on site 2, as well a series of images captured using a GoPro Hero5 Black camera standing on site 3~~.~~ (image resolution of 4000 x 3000 pixels, 12 Mpx). Six LiDAR scans were also taken on site 3. This information was used for quality assessment purposes.

4 Results and discussion

Different results are obtained ~~as a function~~depending on the software used for SfM-MVS processing. For all case studies, VisualSFM gave ~~the best~~ results with print screens from GSV in Google Maps while Agisoft PhotoScan could not align ~~any GSV images from Google Maps~~ those print screens despite adding a series of control points measured with Google Earth Pro. ~~However~~Resolution of print screens images seem to be insufficient to be processed with Agisoft PhotoScan. However, with higher point density and empty areas, Agisoft PhotosScan provided better results with images from Google Earth Pro than VisualSFM.

4.1 Site 1 – “Basse corniche” site

It was possible on “Basse Corniche” site to estimate the fallen volume by scaling and comparing the 2008 ~~and 2010 point clouds. VisualSFM software~~(Figure 4A) and 2010 (Figure 4B) point clouds. The 2008 point cloud is composed of 150’000 points with an average density of 290 points per square meter and the 2014 point cloud is composed of 182’000 points with an average density of 640 points per square meter (Table 1). VisualSFM could align the images and make 3D models before and after the wall collapse. It was possible to roughly scale and georeference the scene with the road width and few point coordinates measured on Google Earth Pro ~~and~~or on the French geoportal ~~(Géoportail, 2016).~~. After aligning the two 3D point clouds, meshes were built to compute the collapsed volume. The point-to-mesh alignment in CloudCompare of both point clouds was done on a small stable part of the cliff~~,~~ (Figure 4C) with a standard deviation of the ~~error below 20 cm (Figure 3C). Not surprisingly, this one is less accurate than other studies using user-end camera and equivalent sensor to object~~point-to-mesh distance ~~(Eltner et al., 2016).~~of about 10 cm (Figure 9 and Table 2) and on the entire cliff beside the vegetation with a standard deviation of about 25 cm (Figure 4E). In the collapsed area, the maximal horizontal distance between the two datasets is about 3.9 m~~.~~ (red colour in Figure 4D). The collapsed volume (including a

~~potentially hole~~possible empty space between the cliff and the wall before the event) was estimated to be about 225 m^3 using the point cloud comparison~~ method described above~~. Based on Google Street images, we manually estimated the dimensions of this volume (15 m long x 10 m high x 1.5 m deep), getting a similar value.

The ~~reasonably good results were~~obtained point clouds on site 1 allow to detect object of few decimetres. This accuracy was adequate to estimate the collapsed volume with an accuracy similar to the estimation made by hand based on the GSV photos and distances measured on Google Earth Pro and the French geoportal. This relatively high accuracy is due to the following factors: good image quality, reduced distance between the cliff ~~proximity to the~~ and camera ~~location, the~~locations, good lighting~~, the~~ conditions, absence of obstacles between the camera location and the ~~wall~~area under investigation, no vegetation and ~~the~~ efficient repartition of point of view around the cliff (Figure 2 A).~~ "Basse Corniche" results (Figure 5 and Table 1) are the best results obtained among the three study areas.~~

4.2 Site 2 – ~~Sechilienne~~Séchilienne Landslide

Eight point clouds of which seven of SfM-MVS process with GSV images were generated for Séchillienne landslide at six different time steps (from April 2010 to June 2015). Three different image sources were used: GSV print screens from Google Maps, GSV images saved from Google Earth Pro and images from a GoPro HERO4+ camera from a moving vehicle (Figure ~~4~~5 and Table 1). Two different programs (VisualSFM and Agisoft PhotoScan) were used for image treatment~~.~~ in function of the image sources (Figure 3 and Table 1). The number of 3D points on the landslide area varies from 9'500 to 22'500 points for a processing with VisualSFM with an average density of 0.25 to 0.85 points per square meter, while 236'000 3D points were generated when using Agisoft PhotoScan~~.~~ with an average density of 2 points per square meter (Table 1). In comparison, 1'500'000 points were obtained on the same area using terrestrial photogrammetry with a 24 Mpx reflex camera. ~~Results were aligned on a 50 cm resolution LiDAR scan of the landslide acquired in 2010. Then, the street view SfM-MVS point clouds were compared with a mesh from the LiDAR scan. The average distance of both point clouds are respectively 0.2 and 1.4 m (distance point to mesh in absolute values). The standard deviations are 1.6 m and 3.8 m (Figure 4 A-E). SfM-MVS point clouds from Google Earth Pro images processed with Agisoft PhotoScan provide the best results (Figure 4G). These images have a resolution about 7.3 times higher than the print screens from Google Maps (1920x1200 pixels for GSV print screens from Google Maps versus 4800x3500 pixels for GSV images exported from Google Earth Pro).~~

~~Landslide changes between 2010 (~~Results were aligned on a 50 cm resolution airborne LiDAR ~~DEM) and 2015 (SfM-MVS) are observable with a material accumulation (red colour in Figure 4G) in the debris cone and some material losses in the upper part~~scan of the landslide ~~(blue colour in Figure 4G). Unfortunately, the back in time function does not exist in Google Earth Pro and it is thus not possible to save old GSV images~~ acquired in 2010. Then, the street view SfM-MVS point clouds were aligned and compared with a mesh from ~~Google Earth Pro. Finally, the comparison between~~ the LiDAR ~~mesh and the SfM-MVS cloud derived from GoPro HERO4+ camera images (Figure 4H) gives similar results to those obtained~~scan using the ~~GSV images from Google Earth Pro (Figure 4G). Thus, the best results of the SVI-derived models were obtained with Agisoft PhotoScan when using Google Earth Pro images. Results were less accurate when using SfM-MVS processing with VisualSFM and lower resolution print screen images from Google Maps.~~

~~This case study shows a good correlation between our ground truth (i.e. LiDAR point cloud) and some SfM-MVS point clouds derived from SVI datasets.~~point-to-mesh strategy. The ~~adjustment~~alignment between the LiDAR point cloud and SfM-MVS point clouds derived from SVI is a key factor ~~defining~~to define the quality of the clouds comparison. This ~~manual adjustment~~alignment on stable areas (manually selected) was not easy to perform because of the low density of points on the SfM-MVS clouds derived from SVI. We noted a huge difference ~~on~~in the number of points between the different SfM-MVS clouds derived from SVI. This difference on the number of points shows the impacts of the image quality. Images with a good quality (resolution, exposition, sharpness) will give point clouds with a higher number of points as point clouds from low quality images.

~~Images~~Comparison results between SfM-MVS point clouds derived from SVI and airborne LiDAR scan highlight surface changes in the Séchilienne landslide over the years (Figure 8 and Table 1). The 2010 point cloud (Figure 5 A2) compared with 2010 LiDAR scan does not show any significant changes. Orange and red colours small dots are spread out on the entire landslide surface suggesting artefacts and not a real slope change. The 2010-2011 point clouds comparison (Figure 5 B2) shows few little red colour pattern (materiel accumulation) in the deposition and in the failure areas. The 2016 point cloud (Figure 5 C2) highlights material deposition in red colour, in the left part. This is confirmed with comparison of a 2013 terrestrial LiDAR. The blue colour pattern indicate a loss of material in the failure and the toe areas. The 2014 point cloud (Figure 5 D2) shows similar results than the 2013 point cloud with however a light increase of material in the deposition area and rock loss in the failure area. The 2010 to 2014 point clouds (Figure 5 A-D) were process with VisualSFM with GSV print screens in Google Maps (Table 1).

Three 2015 point clouds were processed: the first with VisualSFM and GSV print screens (Figure 5E), the second with VisualSFM with GSV images from Google Earth Pro (Figure 5F) and the third with Agisoft PhotoScan with images form Google Earth Pro again (Figure 5G). The results should be the same for the three point clouds but we noticed significant differences. The 2015 point cloud processed with VisualSFM and GSV images from Google Earth Pro (4800 x 3500 pixels), has a higher point density than the 2015 point cloud processed with GSV print screens (1920 x 1200 pixels). The 2015 point cloud with Agisoft PhotoScan and images from Google Earth Pro has a point density significantly higher (Table 1). The accumulation material (red colour in the left part) in the deposition area is clearly observable on the three 2015 point clouds, as the rock displacement-toppling below the failure area (red colour pattern in the failure area viewed as a material accumulation from the road). The loss of material (blue colour) is also well observable in the failure area and, to a lesser extent, in the right part of the deposition area. The last 2015 point cloud is very similar to the 2016 GoPro point cloud (Figure 5 H2) which confirms the results of SfM-MVS processing with GSV images.

Results of site 2 show that images with low resolution and with low lighting generated a lower number of points compared to the models generated with the last generation of GSV cameras, having higher resolution~~ and~~, more advanced sensors and pictures taken with favourable lighting conditions. The large distance between the road and the landslide considerably limits the final accuracy due to low image resolution, as discussed in Eltner et al., ~~2015~~2016; the closest distance between the road and the centre of the landslide is 500 m and the largest distance between the upper part of the landslide and the point of view is about 1’400 m. Furthermore, the vegetation on the landslide foot and along the road as well as a power line partially obstruct the visibility of the study area. In addition, clouds are present on several images on the top of the scarp, degrading the upper part of the 3D point cloud. ~~Results show that it is not possible to bring out changes in the landslide over the years because of the insufficient accuracy of the SfM-MVS point clouds with SVI, except for the 3D clouds resulting from the GSV images saved in Google Earth Pro and processed in Agisoft PhotoScan (Figure 4G). However, the main landslide structures such as little gullies observed in the failure zone and deposition area show an interesting approximation of the current landslide morphology as it was recorded with LiDAR.~~

4.3 Site 3 – Arly Gorges

Four point clouds of which three of SfM-MVS process derived from GSV images were generated on the “Arly gorges” site, at four different times (from March 2010 to December 2016). Three different images sources (GSV print screens from Google Maps, GSV images exported from Google Earth Pro and our own images acquired from a GoPro HERO5 Black) were used (Figure ~~5~~6 and Table 1). Two different programs (VisualSFM and Agisoft PhotoScan) were tested. In addition, a LiDAR point cloud resulting from an assembly of six Optech Ilris scans has been used as ground truth~~.~~ (Figure 6E). The number of points varies from 35’000 points to 3.2 million points with an average density of 40 to 2’200 points per square meter (Table 1).

The 3D point cloud from the “GoPro Hero5 Black” images has been roughly georeferenced, scaled and oriented thanks to the GNSS chip integrated in the camera~~;~~ and has been controlled and refined with points coordinates extracted from Google Maps and the French geoportal. The three point clouds processed from GSV images and the LiDAR scan have been roughly aligned to this reference. Then the four SfM-MVS point clouds (three with GSV images and one with GoPro images) were precisely aligned and scaled on the LiDAR point cloud, which was considered as the reference cloud.

The analysis (Figure 9, Tables 1 and 2) shows that the 2010 model derived from GSV images processed with VisualSFM gives the least accurate results (~~Figure 5A). We~~Figures 6A and 7A): we hardly perceive on that figure the wall of the tunnel entry and the wide cliff structures. The results of the 2014 point cloud from ~~2014~~ GSV images processed with the same program are slightly better (Figure ~~5B).~~6B and 7B): the right-hand tunnel entry is modelled while it was not the case on the 2010 point cloud. The point cloud processed in Agisoft PhotoScan derived from 2016 GSV images saved from Google Earth Pro displays much better quality than the previous (Figure ~~5C). We~~6C and 7C): we now see the protective nets in the slope as well as the blue road sign announcing the tunnel. The vegetation is also observable~~.~~ and the tunnel entry is similarly modelled as the 2016 GoPro point cloud (Figure 6D).

The SfM-MVS point cloud derived from GoPro images gives a significantly better representation of the ~~scene (Figure 5D).~~whole scene, especially on the top of the model. Slope structures and protective nets are well modelled, but not the small vegetation. The comparison between the 2016 LiDAR scan (Figure ~~5E~~6E) and the three SfM-MVS with GSV images point clouds does not allow to identify terrain deformation on the cliff. Moreover, the source area of the rockfall is not observable from the GSV images because it is located higher in the slope, outside of the images.

A great majority of points consistently displayed distances between the LiDAR scan mesh and the SfM-MVS point clouds ranging between +/- 2 m (Figure 5E-5G7 A-C). Protective nets degrade the results because it generates badly modelled surfaces corresponding to the nets on some cliff sections (such as the red-blue section on the top-right of the July 2014 cloud (Figure 5F)).7A)). Considering the tunnel entry (Figure 7 D-F) the average distance point clouds - LiDAR mesh varies from -3 to -6 cm (depends mainly on the alignments of the clouds). Standard deviations vary from 22 cm for the 2010 point cloud to 11 cm for the 2016 point cloud. On a part of the wall above the tunnel (grey colour polygon on Figure 7 D-F), the average distance point cloud - LiDAR mesh varies from -3 cm to -18 cm with standard deviations of 3 cm for the 2010 point cloud, 4 cm for the 2014 point cloud et 6 cm for the 2016 point cloud (Figure 9 and Table 2). We observe again on this site that the improvement of the GSV camera resolution and image quality improve the processing. The information on the pictures source, date, point density and on the program used is given in Table 1.

A strong limiting factor on this site is the non-optimal camera locations. Indeed, the location of the cliff above a tunnel portal does not allow for a lateral movement between the camera positions with regard to the cliff. The maximal viewing angle (in blue colour on the Figure 2A) is about 35° compared to 170° for the site 1, and 115° for the site 2, that is 3 to 5 time smaller than for the other studied sites.

4.4 Discussion

The main limitation found in this study is that SfM-MVS processing is designed to retrieve the internal orientation of standard cameras, whereas the images used in this research do not correspond to a standard camera due the construction of the panoramas. Indeed, the main problem comes from the different deformations on GSV print screens or images due to the panoramas construction. Same strong radial deformations on each images, like on fisheyes images from GoPro cameras, can be processed without limitation with SfM softwares like Agisoft PhotoScan. In addition, images from GSV are often over- or underexposed (case study 3) and their resolution is low for distant subjects (cases study 2 and 3), making difficult to obtain good results with these constraints. Making zoomed print screens from GSV images do not allow increasing the SfM-MVS process results (case study 2) due to a low images resolution. Finally, the spatial repartition of SVI is often problematic because there are not enough images along the track path and because the road path does not often allow obtaining an efficient strategy concerning the camera positions around the studied area (case study 3). Accessing to RAW images together with valuable data of camera calibration would considerably help deriving 3D point clouds from GSV using modern photogrammetric workflows.

Our study highlighted important differences on 3D model reconstruction using different software, consistently with previous works (Micheletti et al., 2015; Gomez-Gutierrez et al., 2015, Niederheiser et al., 2016). Agisoft Photoscan performed better than VisualSFM when using both GSV images from Google Earth Pro (Figure 4F-G) and pictures acquired from a GoPro Hero camera (Figure 4H). Nevertheless, VisualSfM performed better than Agisoft Photoscan on print screens captures from SVI. The only difference between these sources of information is the resolution: 2.3 Mpx for print screens from Google Maps, 16.8 Mpx for images saved from Google Earth Pro and 12Mpx for GoPro camera, stressing the importance of picture resolution on the quality of the 3D model.

With the experience acquired during the research, we can highlight the following recommendations to improve results of SfM-MVS with SVI images. (A) Firstly, the distance between the image point of view and the subject and the size of the subject are important because it influences the pixel size on the subject. In case study case 1, the location of the cliff next to the road (< 1 m) allows to get images with a good resolution for the studied object. In case study case 2, the area under investigation is too far from the road (500 – 1'400 m) and small structures cannot be seen in the landslide. (B) Secondly, the ability to look at the scene from different angles (Figure 2A) is a determining factor to obtain good results. The greater is this "view angle", the better the results will be. Case study 1 with a view angle of almost 180° is optimal because the object is observable from half a circle. View angle of case study 2 (115°) is enough to get many different views of the subject from different angles. The view angle is too narrow to have enough different point of view of the cliff on case study 3 (35°). (C) Thirdly, results are influenced by the image quality and especially by their exposition, contrast and type of sensor, which has progressively been improved during the last years. Image quality varies considerably on different images sets. Case study 1 is again the best study case in term of image quality. Both image sets have optimal solar exposition and shadows are not strong. Case study 2 has sets with very different images quality. Some sets are well exposed, others not. Clouds are present on few image sets. For case study 3, we have a lot of over- and underexposed images on behalf of the situation of the site (incised valley with a southwest oriented slope with a lot of light or shadow). The problem of images quality concerns Google too because it has removed from Google Maps very underexposed GSV images taken in August 2014 on site 3 at the end of 2016.~~ With all these considerations and not surprisingly, the best SfM-MVS results were obtained with the case study 1, whereas the lower quality was obtained at study site 3.~~

According to ~~the results~~our findings, small~~-scale~~ landslides and rockfalls (<~~1~~0.5 m^3) can be detected when the slope or the cliff is close to the road (0-10 m), as it was shown on site 1. Conversely, large slope movements and collapses (>1'000 m^3) can be detected when the studied area is far away from the road (up to 0.5-1 km) like on site 2. On such sites, small changes (<1 m^3) can correspond to either real rockfalls or errors resulting from processing like on the toe of almost all point 3D clouds of Séchilienne landslide (Figure 5 A2-H2). The measured differences between the point clouds on stable areas show ~~good~~interesting results once the point clouds alignment is well done. Thus, we observed standard deviations of ~~a~~few decimetre on stable areas on site 1 (Figure ~~3C~~3D), between 0.5 and 1.1 m on site 2 and between ~~0.1~~11 and ~~0.9~~22 m on the tunnel entry on site 3. Standard deviations increase on site 2 ~~and 3~~ when point clouds are compared on their entire surface (Figure ~~4 A2-H2, Figure~~ 5 ~~E-G and~~A2-H2, Table 1). This is attributable to the occurrence of slope movements generating material increase or decrease and thereby, increasing standard deviations of the ~~error~~distance between the two compared point clouds. It can also be due to a bad 3D point cloud alignment. Indeed, cloud alignment is not always easy on some point clouds because of low point density, because of voids in the point clouds (like in the landslide toe in Figure 5 F2) and because of the roughness of the terrain. In such difficult alignment cases, it was tried to align the point clouds on stable parts where point density was high.

~~4 Conclusion~~

~~The proposed methodology provides interesting but challenging results due to some constraints linked to the SVI. The inconsistent image deformations and the impossibility of extracting the original images from a street view provider are the biggest limitations for 3D model reconstruction derived from SVI. The constraints (distance and obstacles between the studied area and the road, image quality, meteorological conditions, images repartition, number of images, shadows/highlighted areas) strongly limit the proposed approach.~~

~~However, SfM-MVS with SVI can be a useful tool in geosciences to detect and quantify slope movements and displacements at an early stage of the research by comparing datasets taken at different time series. This information is of great interest when no other data of the studied area has been obtained.~~

Our study highlighted important differences on 3D model reconstruction using different software, consistently with previous works (Micheletti et al., 2015; Gomez-Gutierrez et al., 2015, Niederheiser et al., 2016). Agisoft PhotoScan performed better than VisualSFM when using both GSV images from Google Earth Pro (Figure 5F-G) and pictures acquired from a GoPro Hero camera (Figure 5H). Nevertheless, VisualSfM performed better than Agisoft PhotoScan on print screens captures from SVI. The only difference between these sources of information is the resolution: 2.3 Mpx for print screens from Google Maps, 16.8 Mpx for images saved from Google Earth Pro (and 12 Mpx for GoPro camera), stressing the importance of picture resolution on the quality of the 3D model.

The point density was evaluated according to the distance between the image point of view and the subject and the image types and processing software. The obtained results and the derived trends indicate that the use of GSV images from Google Earth Pro with VisualSFM increases by a factor two the point density compared to the processing of GSV print screens with VisualSFM. The processing of GSV images from Google Earth Pro with Agisoft PhotoScan increases by a factor ten the point density compared to the processing of GSV print screens with VisualSFM (trend strips in Figure 8). The expected point density of the 3D point clouds from GSV print screens processed in VisualSFM of a subject located few meters from the camera (“Basse-Corniche” dots on Figure 8) is about 300 points/m^2, about 50 points/m^2 for an area located at about 100 m (“Arly” dots on Figure 8) and about 0.5 point/m^2 for an area located at about 700 m (“Séchilienne” dots on Figure 8).

Despite the above mentioned prospects, some drawbacks were also observed. The main limitation found in this study is that SfM-MVS processing is designed to retrieve the internal orientation of standard cameras, whereas the images used in this research do not correspond to a standard camera due the construction of the panoramas. Indeed, the main problem comes from the different deformations on GSV print screens or images due to the panoramas construction. Same radial deformations, that are stronger than common camera lens, on each images, like on fisheyes images from GoPro cameras, can be processed without limitation with SfM software like Agisoft PhotoScan. In addition, images from GSV are often over- or underexposed (case study 3) and their resolution is low for distant subjects (cases study 2 and 3), making difficult to obtain results with few decimetric accuracy with these constraints. Making zoomed print screens from GSV images do not allow increasing the SfM-MVS process results (case study 2) due to a low images resolution. Finally, the spatial repartition of SVI is often problematic because there are not enough images along the track path and because the road path does not often allow obtaining an efficient strategy concerning the camera positions around the studied area (case study 3). Accessing to original (RAW) images together with valuable data of camera calibration would considerably help deriving 3D point clouds from GSV using modern photogrammetric workflows.

~~The quality of the final product was observed to be mainly dependent on the images quality and of the distance between the studied area and image perspectives. In this study it was possible to detect and characterize small-scale landslides and rockfalls (<1 m^3) for study areas relatively close to the road (from 0 to 10 m); complementarily, it was possible to detect large scale landslides or rock collapses (>1'000 m^3) over areas located far away from the road (hundred meters or more). In other words, it will be difficult, if not impossible, to detect small-scale slope movements of a cliff or a landslide far away from the road with proposed approach.~~

A simple development to improve our proposed approach would be that Google add the *back in time function* into the Google Earth Pro ~~software~~. In this case, it would be possible to save GSV images from any proposed time period and to process those images with Agisoft PhotoScan (Figure ~~4G~~5G) and thus to obtain better results than when using VisualSFM (Figure ~~4F~~5F). Knowing that Google services and functionalities of Google Maps and Google Earth are evolving over time, it is possible that SfM-MVS with GSV images will be more efficient and easier in a near future.

5 Conclusions

In this study it was possible to detect and characterize small landslides and rockfalls (<0.5 m^3) for study areas relatively close to the road (from 0 to 10 m); complementarily, it was possible to detect large scale landslides or rock collapses (>1'000 m^3) over areas located far away from the road (hundred meters or more). This information is of great interest when no other data of the studied area has been obtained.~~Despite of the observed limitations, the~~

The proposed methodology provides interesting but challenging results due to some constraints linked to the quality of the input imagery. The inconsistent image deformations and the impossibility of extracting the original images from a street view provider are the most important limitations for 3D model reconstruction derived from SVI. Following constraints strongly limit the proposed approach: large distances between the camera position and the subject of investigation, presence of obstacles between the studied area and the road, image quality, poor meteorological conditions, non-optimal images repartition, reduced number of images, existence of shadows/highlighted areas. The quality of the final product was observed to be mainly dependent on the images quality and of the distance between the studied area and image perspectives.

Although of the above mentioned limitations, SfM-MVS with SVI can be a useful tool in geosciences to detect and quantify slope movements and displacements at an early stage of the research by comparing datasets taken at different time series. The main interest of the proposed approach is the possibility to use archival imagery and deriving 3D point clouds of an area that has not been captured before the occurrence of a given event. This will allow increasing database on rock slope failures, especially for slope changes along roads which conditions are favourable for the proposed approach.

~~5~~6 References

Abellán, A., Oppikofer, T., Jaboyedoff, M., Rosser, N.J., Lim, M. and Lato, M.J., 2014, Terrestrial laser scanning of rock slope instabilities. Earth Surface Processes and Landforms, v. 39, p.80-97.

Agisoft, L. L. C., 2015, Agisoft PhotoScan user manual, Professional edition, version 1.2.6.

Anguelov, D., Dulong, C., Filip, D., Frueh, Ch., Lafon, S., Lyon, R., Ogale, A., Vincent, L., Weaver, J., 2010, Google Street View: Capturing the world at street level. Computer, Vol. 43, IEEE, 32-38.

Carrivick, J. L., Smith, M. W., Quincey, D. J., 2016, Structure from Motion in the Geosciences. John Wiley & Sons.

Dubois, L., Chanut, M.-A., Duranthon, J.-P., 2014, Amélioration continue des dispositifs d'auscultation et de surveillance intégrés dans le suivi du versant instable des Ruines de Séchilienne. Géologues n°182, p50-55.

Durville, J.-L., Bonnard, C., Potherat, P., 2011, The Séchilienne (France) landslide: a non-typical progressive failure implying major risks, Journal of Mountain Science, Vol. 8, Issue 2, 117-123.

Eltner, A., Kaiser, A., Castillo, C., Rock, G., Neugirg, F. and Abellán, A., 2016, Image-based surface reconstruction in geomorphometry–merits, limits and developments. Earth Surface Dynamics, 4(2), pp.359-389.

Favalli, M., Fornaciai, A., Isola, I., Tarquini, S., Nannipieri, L., 2011, Multiview 3D reconstruction in geosciences, Computers & Sciences 44, 168-176.

Fey, C., Wichmann, V., 2016, Long-range terrestrial laser scanning for geomorphological change detection in alpine terrain – handling uncertainties. Earth Surf. Process. Landforms.

Fernández, T., Pérez, J. L., Cardenal, J., Gómez, J. M., Colomo, C., Delgado, J., 2016, Analysis of Landslide Evolution Affecting Olive Groves Using UAV and Photogrammetric Techniques. Remote Sensing, 8(10), 837.

Furukawa, Y., Ponce, J., 2010, Accurate, dense, and robust multiview stereopsis. Pattern Analysis and Machine Intelligence, IEEE Transactions on, 32(8), 1362-1376.

Furukawa, Y., Curless, B., Seitz, S. M., Szeliski, R., 2010, Towards internet-scale multi-view stereo. In Computer Vision and Pattern Recognition (CVPR), 2010 IEEE Conference on (pp. 1434-1441). IEEE.

France 3 : Important éboulement dans les gorges de l'Arly en Savoie, 2014, available at : http://france3-regions.francetvinfo.fr/alpes/savoie/important-eboulement-dans-les-gorges-de-l-arly-en-savoie-400849.html (last access 25 January 2017).

Géoportail, IGN (2016), 2016, available at http://www.geoportail.gouv.fr (last access 25 January 2017).

Girardeau-Montaut, D., 2011, CloudCompare-Open Source project. OpenSource Project.

Gómez-Gutiérrez, Á., de Sanjosé-Blasco, J.J., Lozano-Parra, J., Berenguer-Sempere, F. and de Matías-Bejarano, J., 2015, Does HDR pre-processing improve the accuracy of 3D models obtained by means of two conventional SfM-MVS software packages? The case of the Corral del Veleta Rock Glacier. Remote Sensing, 7(8), pp.10269-10294.

Google Street View, Understand Street View, 2017, available at https://www.google.com/maps/streetview/understand (last access 25 January 2017).

Google Maps, Google Inc. (2017), 2017, available at https://maps.google.com (last access 25 January 2017).

Google Earth Pro, version 7.1.2.241, Google Inc. (2013), 2013, available at https://www.earth.google.com/earth (last access 25 January 2017).

Guerin, A., Abellán, A., Matasci, B., Jaboyedoff, M., Derron, M.-H., and Ravanel, L.: Brief communication: ~~3D~~3-D reconstruction of a collapsed rock pillar from ~~web~~Web-retrieved images and terrestrial ~~LiDAR~~lidar data – ~~The~~the 2005 event of the ~~West~~west face of the Drus (Mont-~~-~~ Blanc massif), Nat. Hazards Earth Syst. Sci~~. Discuss., ~~., 17, 1207-1220, https://doi~~:~~.org/10.5194/nhess-~~2016-316, in review, 2016~~17-1207-2017, 2017.

James, M. R., Robson, S., 2012, Straightforward reconstruction of 3D surfaces and topography with a camera, Accuracy and geosciences application, Journal of Geophysical research, Vol. 117, F03017.

Klingner, B., Martin, D., Roseborough, J., 2013, Street View Motion-from-Structure-from-Motion, Proceedings of the International Conference on Computer Vision, IEEE.

Kromer, R., Abellán, A., Hutchinson, J., Lato, M., Edwards, T., Jaboyedoff, M., 2015, A 4D Filtering and Calibration Technique for Small-Scale Point Cloud Change Detection with a Terrestrial Laser Scanner. Remote Sensing vol.7, pp.13029-13052; DOI: 10.3390/rs71013029.

Lichtenauer, J. F., Sirmacekb, B., 2015, A semi-automatic procedure for texturing of laser scanning point with google streetview images, The International Archives of the Photogrammetry, Remote Sensing and Spatial Information Sciences, Volume XL-3/W3, 109-114.

Le Roux, O., Schwartz, S., Gamond, J. F., Jongmans, D., Bourles, D., Braucher, R., Mahaney, W., Carcaillet, J., Leanni, L., 2009, CRE dating on the head scarp of a major landslide (Séchilienne, French Alps), age constraints on Holocene kinematics, Earth and Planetary Science Letters, Vol. 280, 236-245.

Lucieer, A., de Jong, S., Turner, D., 2013, Mapping landslide displacements using Structure from Motion (SfM) and image correlation of multi-temporal UAV photography, Progress in Physical Geography, Vol. 38(1), 97-116.

Luhmann, T., Robson, S., Kyle, S., Boehm, J., 2014, Close-range photogrammetry and 3D imaging. Walter de Gruyter.

Lowe, D., 1999, Object recognition from local scale-invariant features. International Conference of Computer Vision, Corfu Greece, 1150-1157.

Luhmann, T., Robson, S., Kyle, S., Boehm, J., 2014, Close-range photogrammetry and 3D imaging, Walter De Gruyter.

Micheletti, N., Chandler, J. H., Lane, S. N., 2015, Investigating the geomorphological potential of freely available and accessible Structure-from-Motion photogrammetry using a smartphone. Earth Surface Processes and Landforms, Vol 40(4), 473-486.

Nice-Matin : La basse corniche coupée en direction de Monaco après un éboulement, 2014, available at : http://www.nicematin.com/menton/la-basse-corniche-coupee-en-direction-de-monaco-apres-un-eboulement.1587292.html (last access 15 October 2015).

Niederheiser, R., Mokroš, M., Lange, J., Petschko, H., Prasicek, G., & Elberink, S. O., 2016, Deriving 3d Point Clouds from Terrestrial Photographs-Comparison of Different Sensors and Software. International Archives of the Photogrammetry, Remote Sensing and Spatial Information Sciences-ISPRS Archives, 41, 685-692.

Oppikofer, T., Jaboyedoff, M., Blikra, L., Derron, M.-H., Metzger, R., 2009, Characterization and monitoring of the Åknes rockslide using terrestrial laser scanning. Natural Hazards and Earth System Science 9: 1003–1019.

Rosser, N.J., Petley, D.N., Lim, M., Dunning, S.A., Allison, R.J., 2005, Terrestrial laser scanning for monitoring the process of hard rock coastal cliff erosion. Quarterly Journal of Engineering Geology and Hydrogeology 38(4): 363–375.

Royán, M.J., Abellán, A., Jaboyedoff, M., Vilaplana, J. M., Calvet, J.,2014, Spatio-temporal analysis of rockfall pre-failure deformation using Terrestrial LiDAR. Landslides, pp.1–13.

Ruggles, S., Clark, J., Franke, K. W., Wolfe, D., Reimschiissel, B., Martin, R. A., ... & Hedengren, J. D.,2016, Comparison of SfM computer vision point clouds of a landslide derived from multiple small UAV platforms and sensors to a TLS-based model. Journal of Unmanned Vehicle Systems, 4(4), 246-265.

Snavely, N., M. Seitz, S., Szeliski, R., 2006, Photo Tourism: Exploring Photo Collection in 3D. In SIGGRAPH 06, 835-846.

Snavely, N., 2008, Scene reconstruction and visualization from Internet photo collections, unpublished PhD thesis, University of Washington, USA.

Snavely, N., Seitz, S., Szeliski, R., 2008, Modeling the World from Internet Photo Collections Int J Comput Vision, Springer Netherlands, 80, 189-210

Streetside, Microsoft Inc. (2017), 2017, available at https://www.microsoft.com/maps/streetside.aspx (last access 25 January 2017).

Stumpf, A., Malet, J. P., Allemand, P., Pierrot-Deseilligny, M., Skupinski, G., 2015, Ground-based multi-view photogrammetry for the monitoring of landslide deformation and erosion. Geomorphology, 231, 130-145.

Tencent Maps, Tencent Inc. (2017), 2017, available at http://map.qq.com (last access 25 January 2017).

Turner, D., Lucieer, A., Watson, C., 2012, An Automated Technique for Generating Georectified Mosaics, from Ultra-High Resolution Unmanned Aerial Vehicle (UAV), Conference on 3D Imaging, Modeling, Processing, Visualization & Transmission Imagery, Based on Structure from Motion (SfM) Point Clouds, Remote Sensing, 4(5), 1392-1410 IEEE,479-486.

Walstra, J., Chandler, J. H., Dixon, N., Dijkstra, T. A., 2007, Aerial photography and digital photogrammetry for landslide monitoring. Geological Society, London, Special Publications, 283(1), 53-63.

Wang, C.-P., Wilson, K., Snavely, N., 2013, Accurate Georegistration of Point Clouds Using Geographic Data, In 3D Vision – 3DV, IEEE, 33-40.

Westoby, M.J., Brassington, J., Glasser, N.F., Hambrey, M.J., Reynolds, J.M., 2012, 'Structure-from-Motion' photogrammetry: A low-cost, effective tool for geoscience applications, Geomorphology, Vol. 179, 300-314.

Wu, C., 2011, VisualSFM: A visual structure from motion system, available at http://ccwu.me/vsfm (last access 25 January 2017).

Zamir, A. R., Shah, M., 2010, Accurate Image Localization Based on Google Maps Street View, In Computer Vision – ECCV 2010, Springer, 255-268.

~~6~~7 Figures

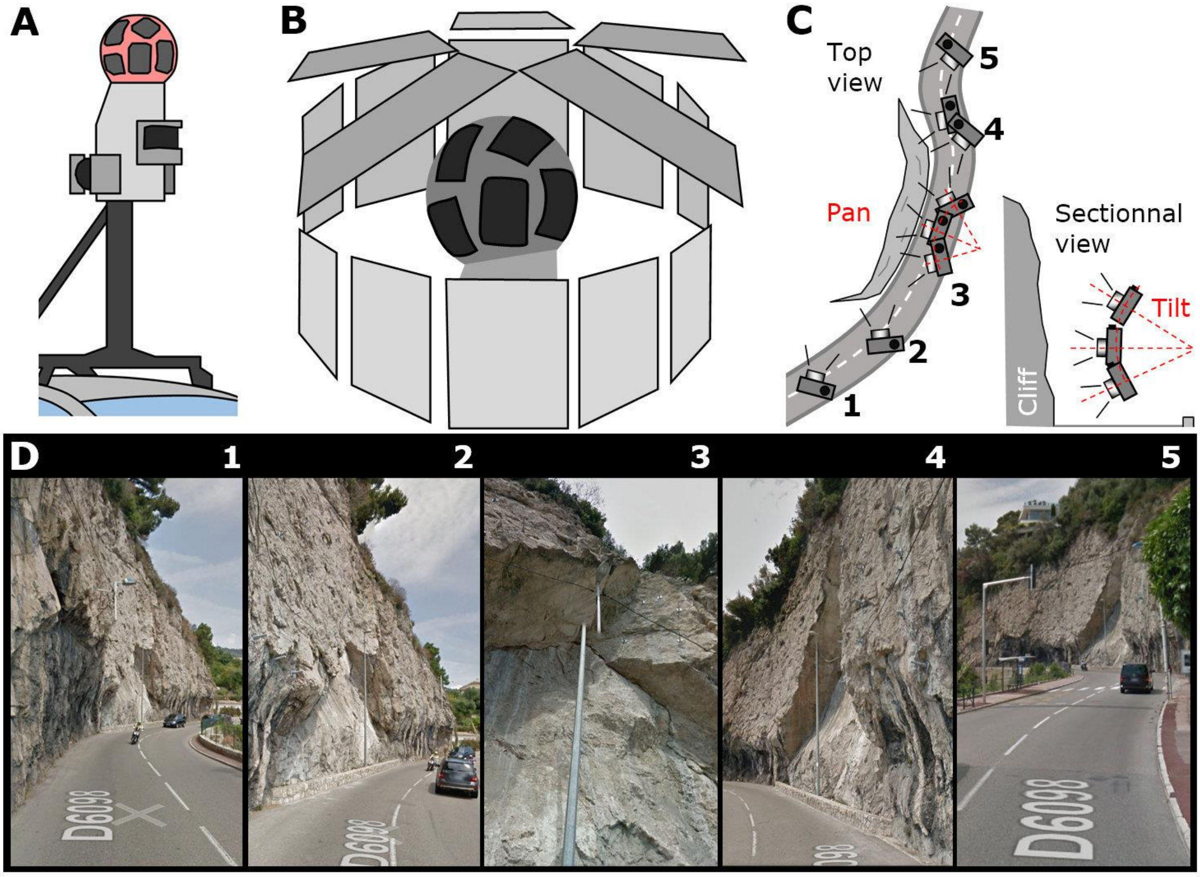

Figure 1: Google Street View (GSV) imagery functioning. A: Schema of the GSV spherical camera system mounted on a car roof. Sensors in black colour are LiDAR on which are draped the GSV images (based on Google Street View 2017). B: Functioning of the GSV spherical panorama built with fifteen images. C: Strategy of the GSV service for SfM-MVS photogrammetry. Numbers correspond schematically to the images in D. D: Screen captures of GSV photos from the study site 1. The image numbers correspond to those in C. Note the gap on the street-lamp in images 3 due to the panorama construction from the GSV pictures.

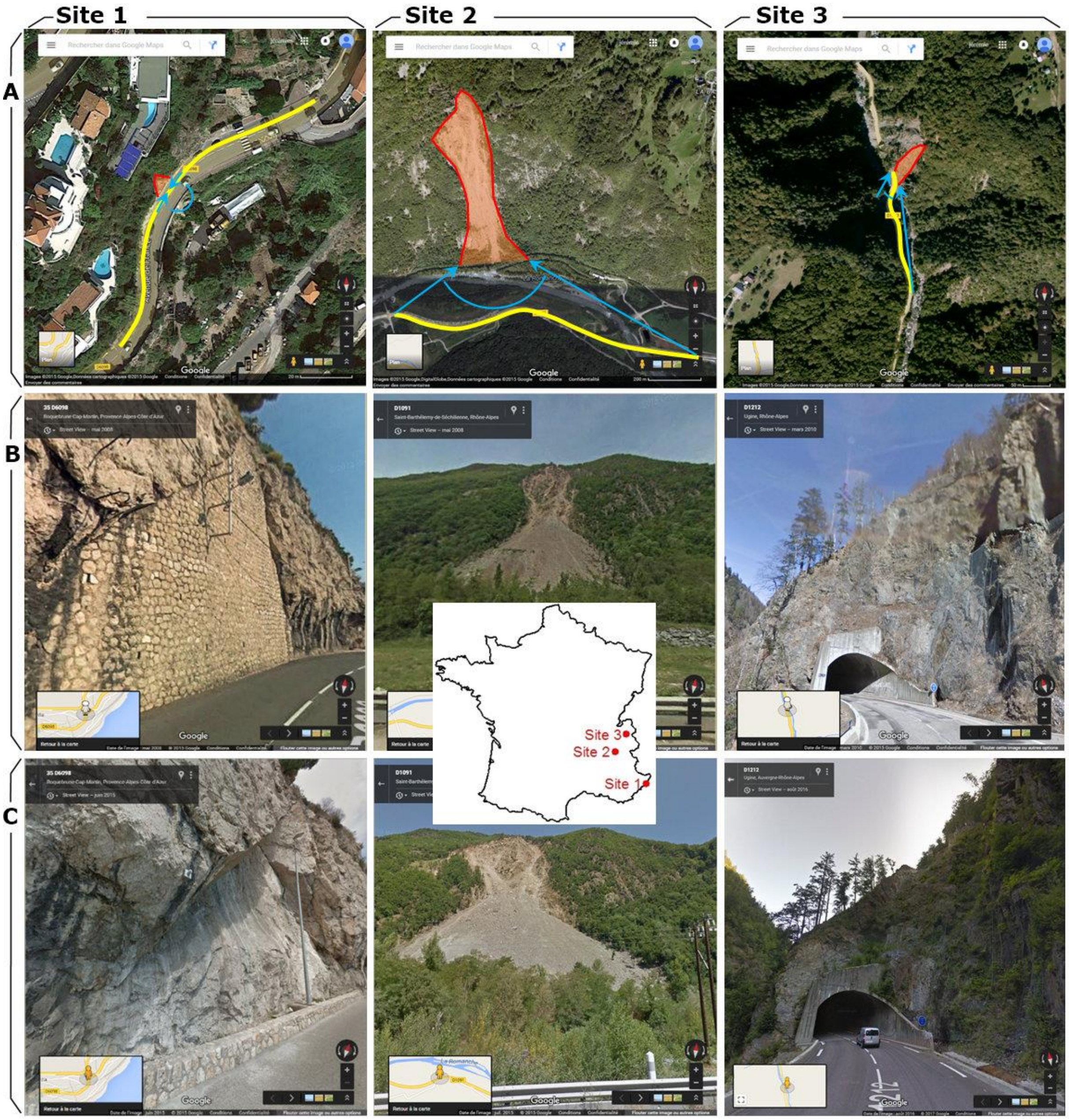

Figure 2 : The three French studied sites (1: Basse-Corniche, 2: Séchilienne and 3: Arly gorges). A: Google Maps aerial view of the sites (in red) with the road path (yellow) used to take the GSV images of the scenes and the view angle (blue) of the images point of view around the sites. B: First GSV of the sites. C: Last GSV of the sites.

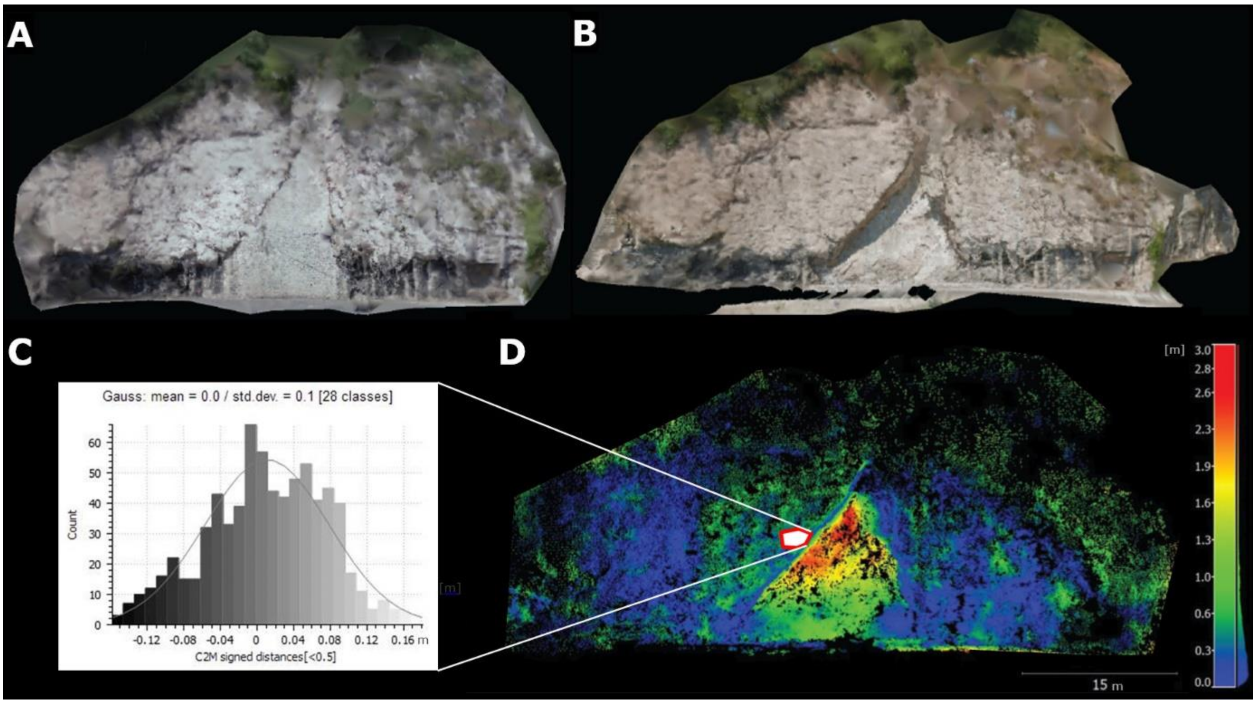

Figure 3 : Results at site 1 “BAsse-Corniche”.

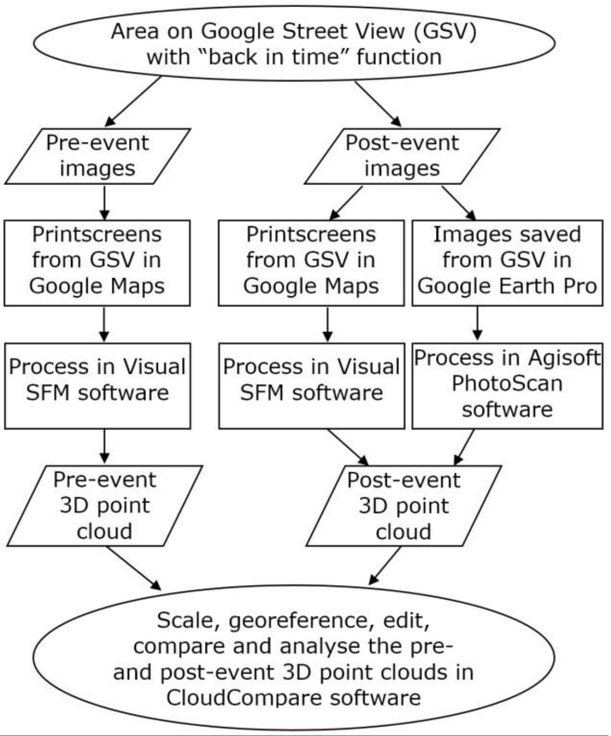

Figure 3: Flowchart of the SfM-MVS processing with GSV images on an area with the "back in time" function available. Pre-event images are displayed using the "back in time" function in GSV. Post-event images arise either from print screens of GSV in Google Maps using or not the "back in time" function or from GSV images saved in Google Earth Pro. In this last case, the last available proposed GSV images have a greater resolution as the print screens and can be processed in the Agisoft PhotoScan.

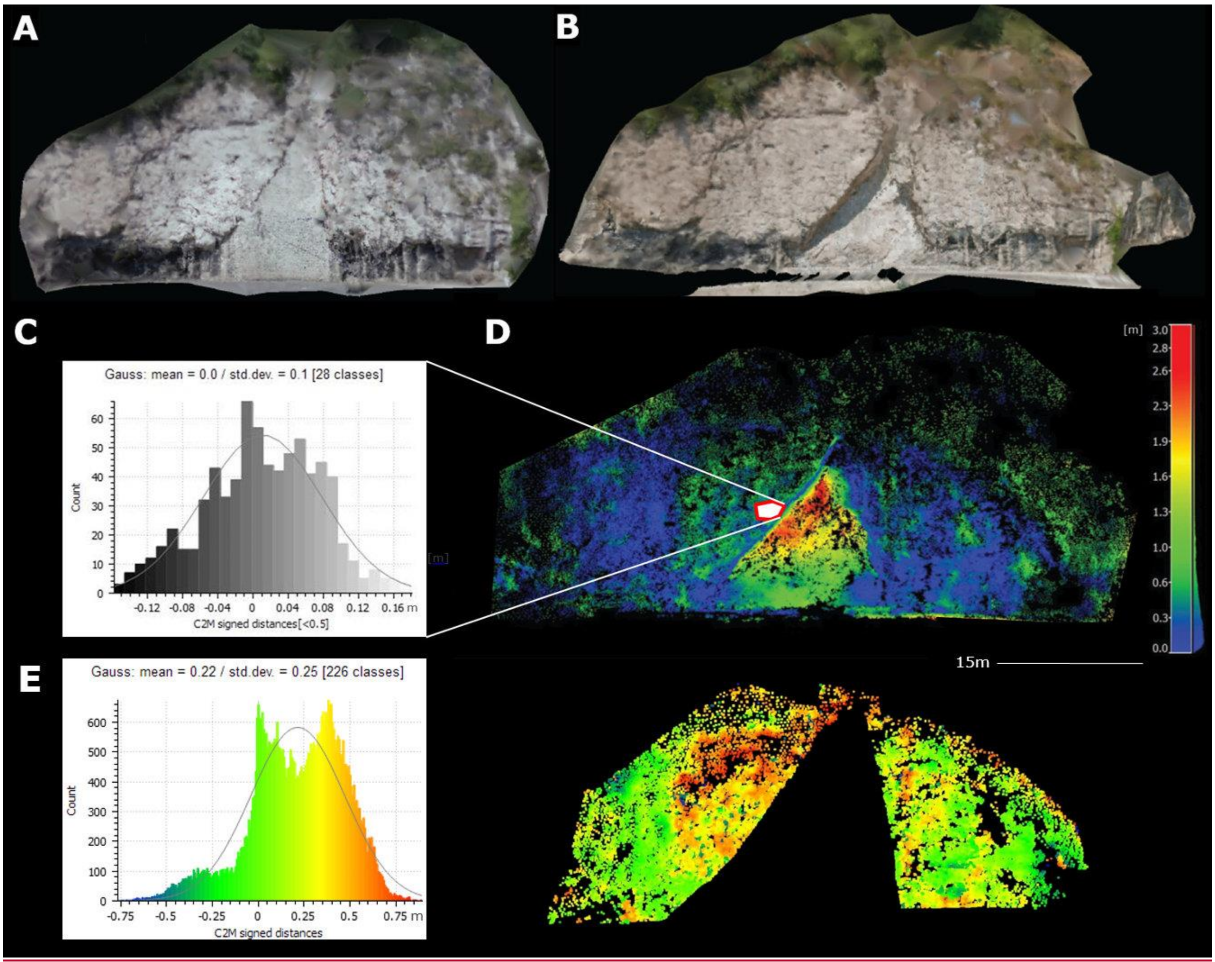

Figure 4: Results at site 1 “Basse-Corniche”. A: 3D model produced with GSV images taken before the event in 2008. B: 3D model produced with GSV images taken after the event in 2014. C: Statistics on a small part of the wall (red colour polygon on figure D) of 7’510 points between the two point clouds~~.~~ with the point-to-mesh strategy in the CloudCompare. D: Comparison of the two point clouds of 2008 and 2014~~.~~ on the entire surface of the 3D point clouds. The maximal horizontal depth of the cliff is about 3.9 m. E: Comparison of the two point clouds of 2008 and 2014 on the entire stable parts of the cliff (i.e. without vegetation) by not taking into account the collapsed wall (black triangle in the centre of the point clouds. The information on the pictures source~~ and~~, date, point density and on the program used is given in ~~Table~~Tables 1 and 2.

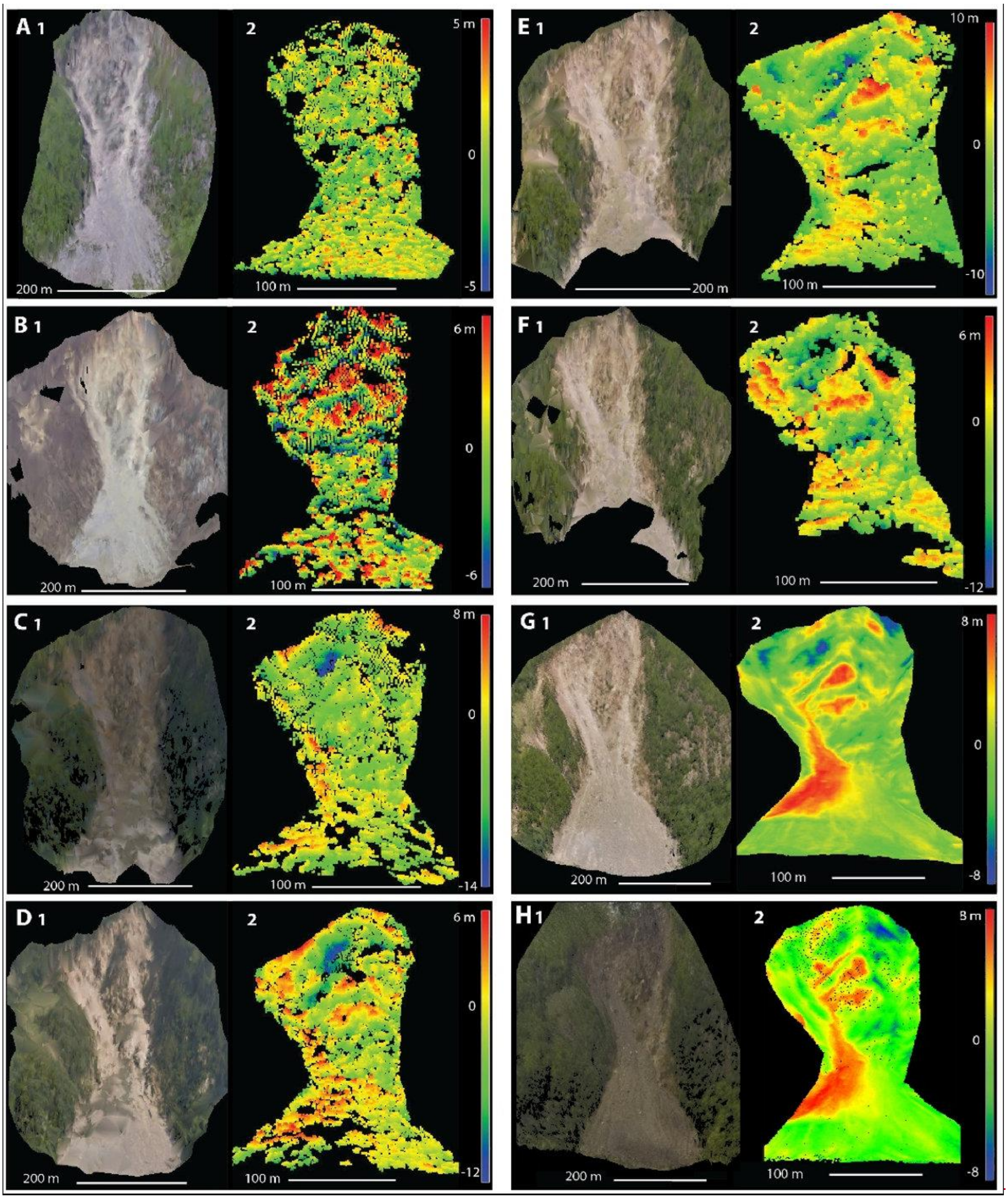
A 1
200 m
2
5 m
0
-5
100 m
E 1
200 m
2
10 m
0
-10
100 m
B 1
200 m
2
6 m
0
-6
100 m
F 1
200 m
2
6 m
0
-12
100 m
C 1
200 m
2
8 m
0
-14
100 m
G 1
200 m
2
8 m
0
-8
100 m
D 1
200 m
2
6 m
0
-12
100 m
H 1
200 m
2
8 m
0
-8
100 m

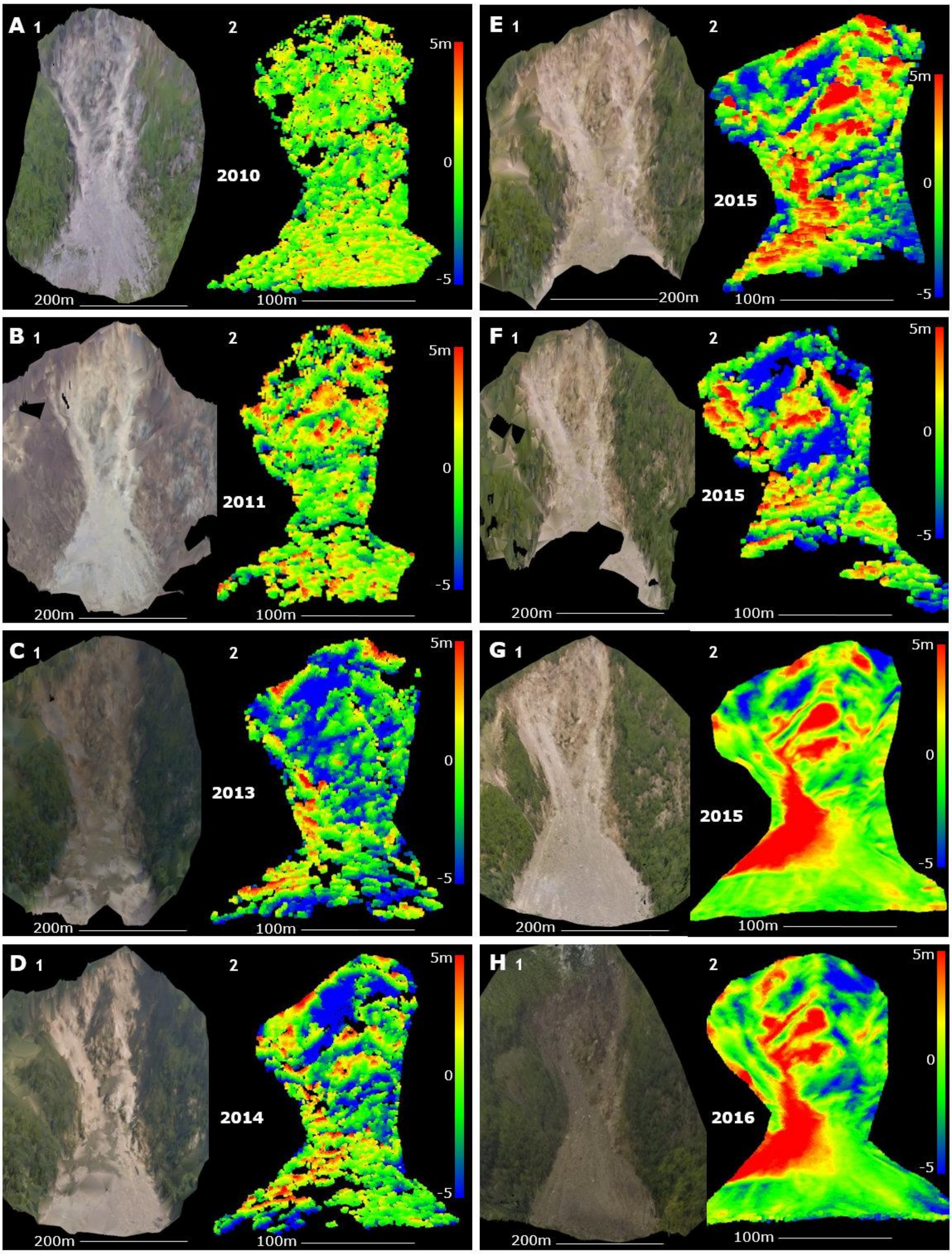

Figure 45 : Results at site 2 "Séchilienne". Eight points clouds from different images sets taken at six different time with three different image sources and processed with two different programs. Figures A1-H1: Meshs resulting from the respective point clouds. Figures A2-H2: point clouds comparison with a 50 cm LiDAR DEM from 2010 (red colour points is material increase; blue colour points are material decrease from the 2010 LiDAR cloud).) with the point-to-mesh strategy in CloudCompare. The information on the pictures source and, date, point density and on the program used is given in Table 1.

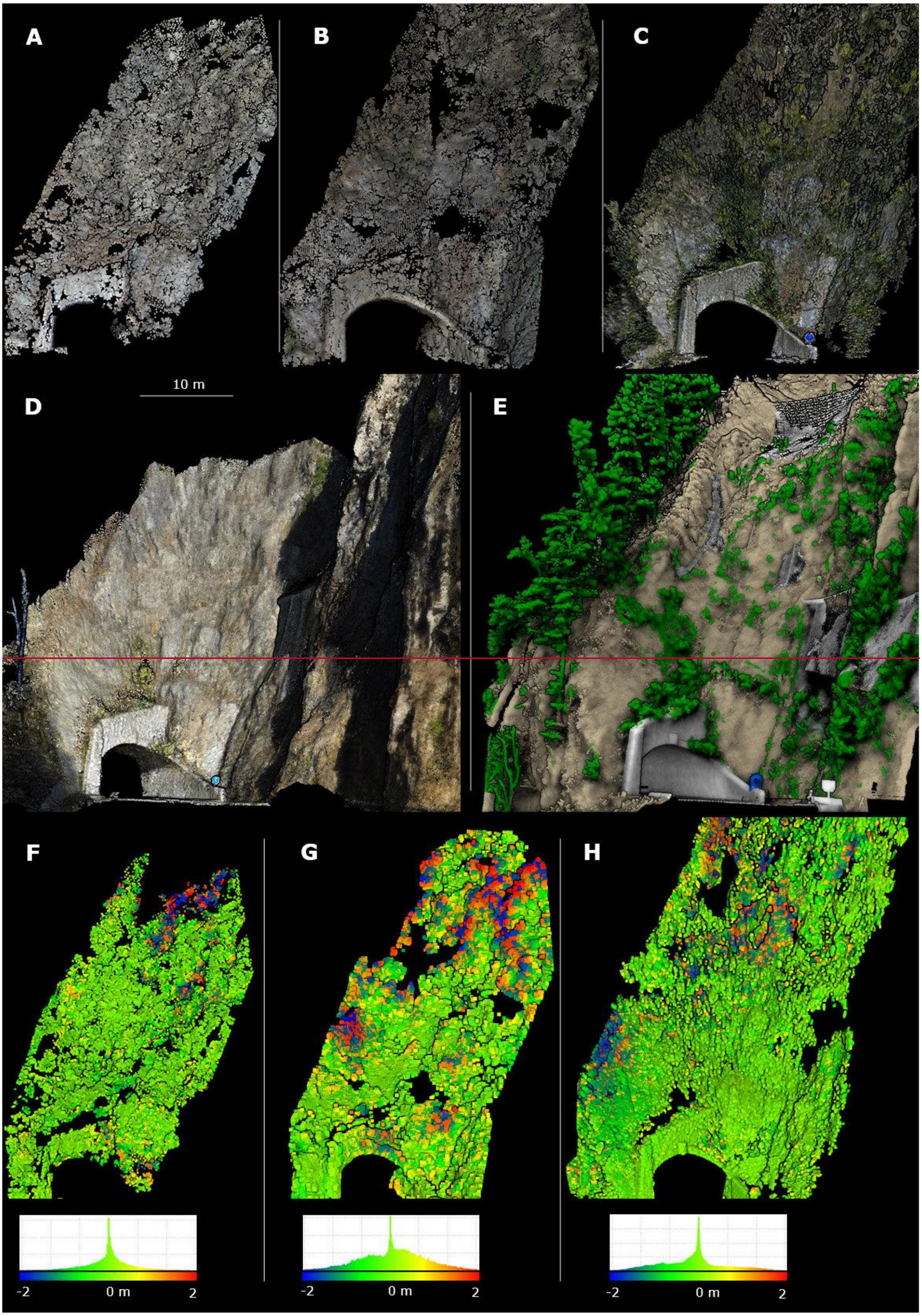
A
B
C
10 m
D
E
F
G
H
-2
0 m
2
-2
0 m
2
-2
0 m
2

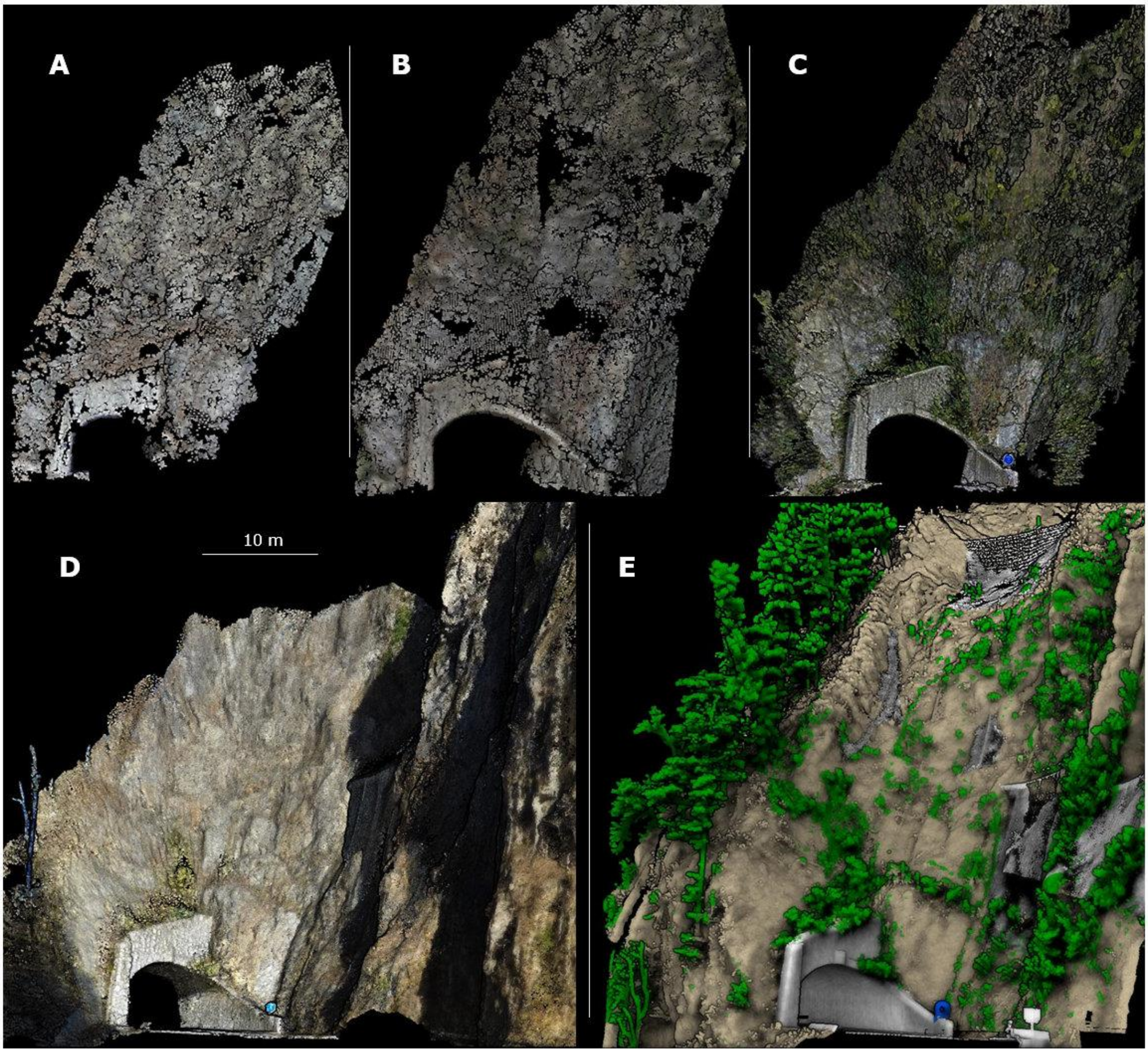

Figure ~~5~~6 : Results at site 3 "Arly gorges". Five points clouds from four different images sets sources and processed with two different softwares and one LiDAR scan. A: March 2010 point cloud. B: July 2014 point cloud. C: August 2016 point cloud. D: December 2016 point cloud taken on foot with a GoPro camera. E: December 2016 LiDAR cloud from an assembly of six Optech terrestrial LiDAR scans. The grey elements in the cliff are the protective nets. ~~F G H~~

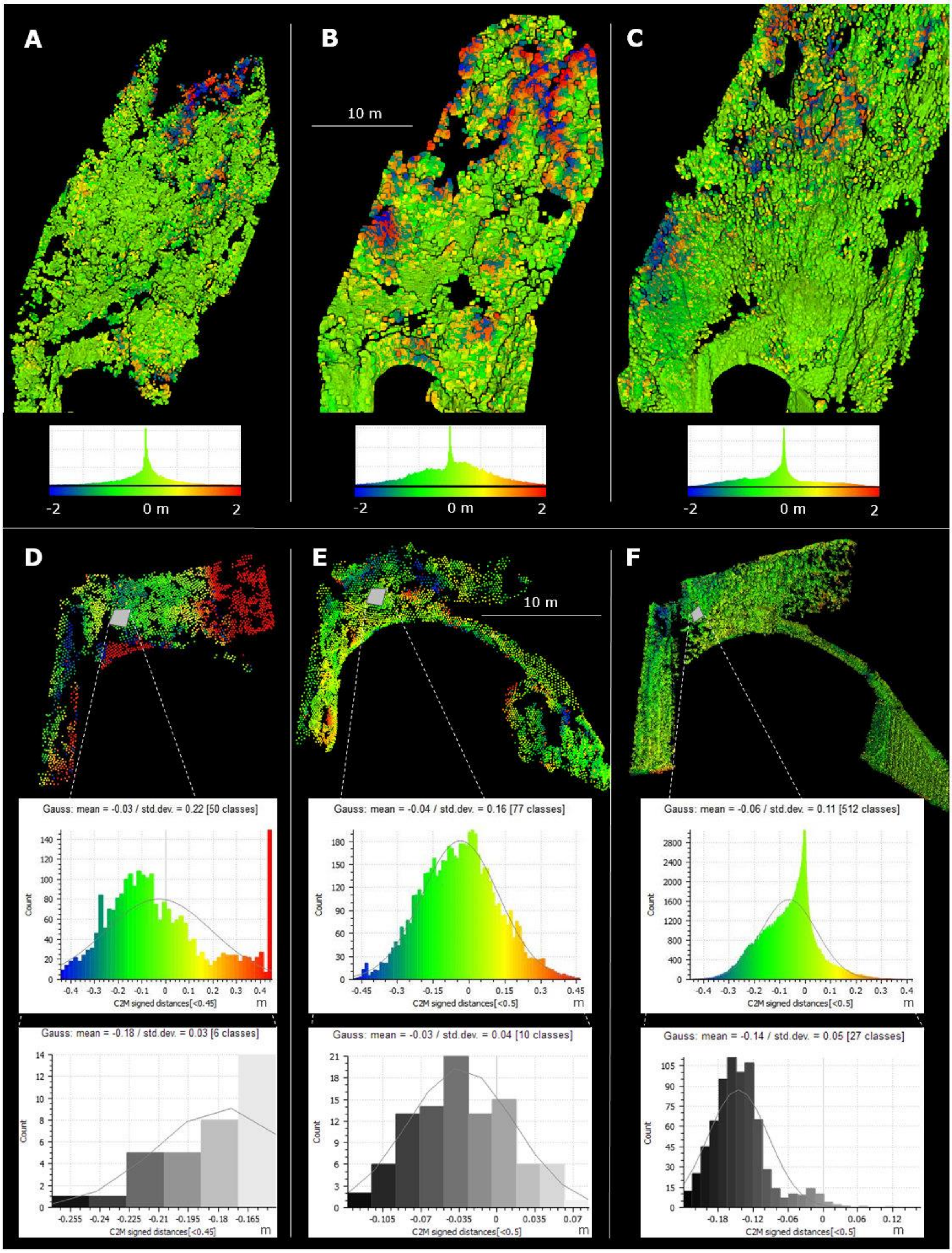

Figure 7: A-B-C: March 2010, July 2014 and August 2016 point clouds compared with December 2016 LiDAR DEM (red colour points is material increase; blue colour points are material decrease from the 2016 LiDAR cloud).) with the point-to-mesh strategy on the CloudCompare. D, E, F: tunnel entry and part of the wall overlooking the tunnel (grey colour polygon) of the March 2010, July 2014 and August 2016 point clouds compared with December 2016 LiDAR DEM. The information on the pictures source and, date, point density and on the program used is given in TableTables 1 and 2.

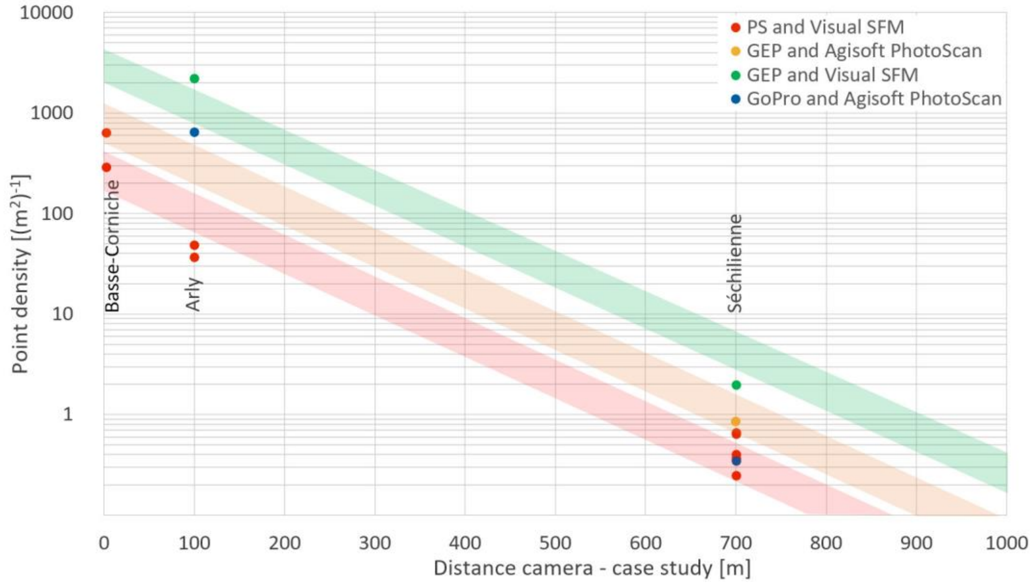

Figure 8: Correlation between distance camera - case studies and the expected density of points from the three case studies. The red colour dots are results of the three case studies point clouds obtained from Google Street View (GSV) print screens (PS) in Google Maps (GM) processed with VisualSFM. The red strip represents the corresponding trend based on a negative exponential function. The orange colour dot is the result of the Séchilienne point cloud obtained from GSV images saved in Google Earth Pro (GEP) processed with VisualSFM. The orange strip represents the corresponding trend based on a negative exponential function. The green colour dots are results of the Séchilienne and Arly point clouds obtained from GSV images saved in (GEP) processed with Agisoft PhotoScan. The green strip represents the corresponding trend based on a negative exponential function. By way of comparison, the blue colour dots represent the result of the Séchilienne and Arly point clouds obtained with GoPro action camera images taken on the field and processed with Agisoft PhotoScan.

Figure 9: Correlation between distance camera - case studies and the expected standard deviation from the three case studies. The dots are results of point clouds comparisons on the entire point cloud areas (Table 1). The triangle are results of point clouds comparisons on partial point cloud area (Table 2). The red colour dots and triangle are results of the three case studies point clouds obtained from Google Street View (GSV) print screens (PS) in Google Maps (GM) processed with VisualSFM compared on the entire area. The orange colour dot is the result of the Séchilienne point cloud obtained from GSV images saved in Google Earth Pro (GEP) processed with VisualSFM. The green colour dots and triangles are results of the Séchilienne and Arly point clouds obtained from GSV images saved in (GEP) processed with Agisoft PhotoScan. By way of comparison, the blue colour dots represent the result of the Séchilienne and Arly point clouds obtained with GoPro action camera images taken on the field and processed with Agisoft PhotoScan.

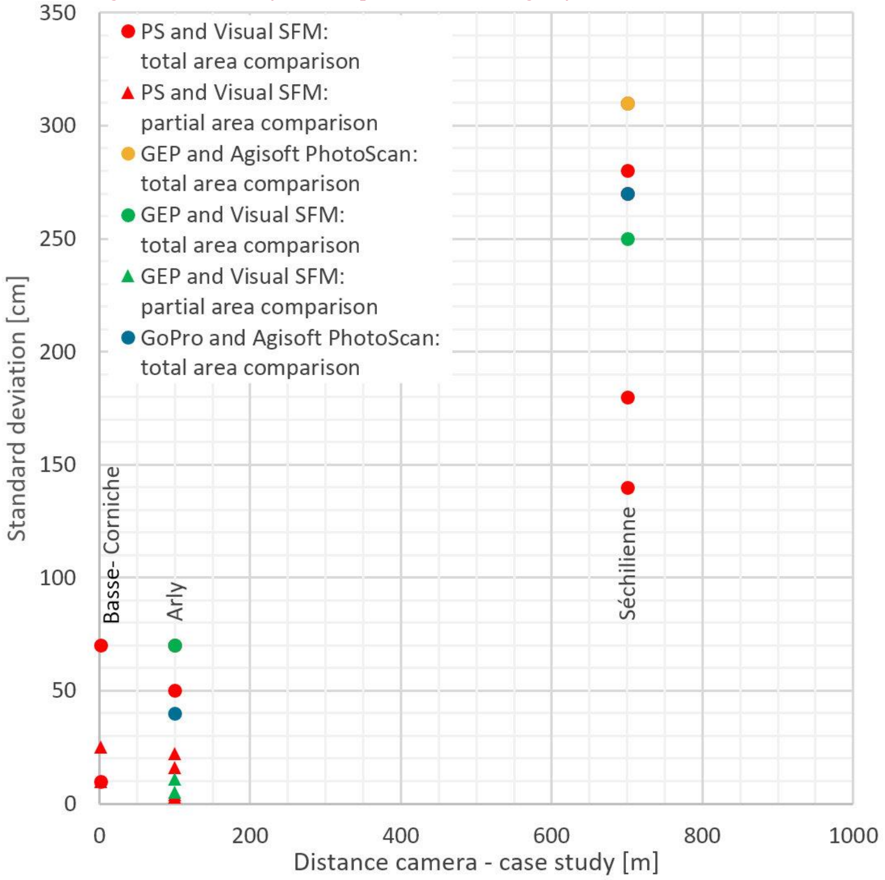

Table 1: List of the fourteen point clouds presented in this paper.

Site	Figure	Date	Images source	Images size [pixel]	Images number	Point density[1] (pts/m²)	Processing software	Number of points	Comparison: With			Min.Mean distance[2] [m]	Max. [m]	Average [m]	Std. dev. [m]
Site 1	Fig. 3A4A	2008.05	PS GSV, GM[1] from GM[3]	1920 x 1200	60	290	VisualSFM	150'000	14.06[5]0	-1.2	2.6	0.2			0.7
	Fig. 3B4B	2014.06	PS GSV, GM[1] from GM[3]	1920 x 1200	50	640	VisualSFM	182'000	8.05[6]05[8]			-0.20	0.2	0	0.1
Site 2	Fig. 4A5A	2010.04	PS GSV, GM[1] from GM[3]	1920 x 1200	54	0.40	VisualSFM	18'000	DAR[7]LiR[9]	-5.5	4.9	-0.2			1.4
	Fig. 4B5B	2011.03	PS GSV, GM[1] from GM[3]	1920 x 1200	52	0.25	VisualSFM	9'500	DAR[7]LiR[9]	-6.6	6.8	-0.1			1.8
	Fig. 4C5C	2013.05	PS GSV, GM[1] from GM[3]	1920 x 1200	45	0.37	VisualSFM	12'500	DAR[7]LiR[9]	-13.9	7.9	-2.1			2.7
	Fig. 4D5D	2014.06	PS GSV, GM[1] from GM[3]	1920 x 1200	52	0.66	VisualSFM	25'000	DAR[7]LiR[9]	-12.8	6.3	-1.5			2.8
	Fig. 4E5E	2015.06	PS GSV, GM[1] from GM[3]	1920 x 1200	62	0.64	VisualSFM	23'500	DAR[7]LiR[9]	-11.4	9.7	-0.9			3.1
	Fig. 4F5F	2015.06	GSV, GEP[2] from GEP[4]	4800 x 3500	80	0.86	VisualSFM	22'500	DAR[7]LiR[9]	-11.9	7.4	-1.7			3.1
	Fig. 4G5G	2015.06	GSV, GEP[2] from GEP[3]	4800 x 3500	80	1.99	Agisoft PhotoScan	236'000	DAR[7]LiR[9]	-8.1	8.3	0.6			2.5
	Fig. 4H5H	2016.05	GoPro[3]GoPro[5]	4000 x 3000	75	0.35	Agisoft PhotoScan	46'000	DAR[7]LiR[9]	-8.9	8.1	-0.2			2.7
Site 3	Fig. 5A, 5FFigs. 6A, 7A	2010.03	PS GSV, GM[1] from GM[3]	1920 x 1200	66	40	VisualSFM	35'000	DAR[8]LiR[10]	-2.2	2.1	0.0			0.5
	Fig. 5B, 5GFigs. 6B, 7B	2014.07	PS GSV, GM[1] from GM[3]	1920 x 1200	111	50	VisualSFM	53'000	DAR[8]LiR[10]	-2.2	2.3	0.1			0.7
	Fig. 5C, 5HFigs. 6C, 7C	2016.08	GSV, from GEP[2]	4800 x 3107	64	2200	Agisoft PhotoScan	3'1850'000	DAR[8]LiR[10]	-2.3	2.5	-0.1			0.7
	Fig. 5D6D	2016.12	GoPro[4]GoPro[6]	4000 x 3000	50	650	Agisoft PhotoScan	2'217'000	DAR[8]LiDAR[10]			-4.20	3.4	0	0.4

[1] Point density around a search radius of 2 m.
[2] Average distance between the mesh of the reference point cloud and the compared point cloud using the point-to-mesh strategy.
[3] Print screens (PS) of Google Street View (GSV) from Google Maps (GM).
[24] Google Street View (GSV) images saved in Google Earth Pro (GEP).
[35] GoPro Hero4+.
[46] GoPro Hero5 Black with GNSS chip integrated.
[57] Comparison between the entire point clouds of May 2008 and June 2014 (Figure 3D).
[68] Comparison of a small cliff area of the May 2008 and June 2014 point clouds (Figure 3C).
[79] Comparison with the 50 cm airborne LiDAR DEM from 2010.
[810] Comparison with the December 2016 LiDAR DEM (6'930'000 points) without vegetation from an assembly of six Optech terrestrial LiDAR clouds.

Table 2: List of the eight partial point cloud comparisons.

Site	Figure	Date	Images source	Images size [pixel]	Processing software	Comparison: Comparative area	With	Mean distance[1] [cm]	Std. dev. [cm]
Site 1	Fig. 4C	2008.05	PS GSV from GM[2]	1920 x 1200	VisualSFM	Small cliff part	4.06[4]	0	10
	Fig. 4E	2008.05	PS GSV from GM[2]	1920 x 1200	VisualSFM	Entire cliff without wall and vegetation	4.06[4]	22	25
Site 3	Fig. 7D 1	2010.03	PS GSV from GM[2]	1920 x 1200	VisualSFM	Tunnel entry	)AR[5]	-3	22
	Fig. 7D 2	2010.03	PS GSV from GM[2]	1920 x 1200	VisualSFM	Small part of tunnel entry	)AR[5]	-18	3
	Fig. 7E 1	2014.07	PS GSV from GM[2]	1920 x 1200	VisualSFM	Tunnel entry	)AR[5]	-4	16
	Fig. 7E 2	2014.07	PS GSV from GM[2]	1920 x 1200	VisualSFM	Small part of tunnel entry	)AR[5]	-3	4
	Fig. 7F 1	2016.08	GSV from GEP[3]	4800 x 3107	Agisoft PhotoScan	Tunnel entry	)AR[5]	-6	11
	Fig. 7F 2	2016.08	GSV from GEP[3]	4800 x 3107	Agisoft PhotoScan	Small part of tunnel entry	)AR[5]	-14	5

[1] Average distance between the mesh of the reference point cloud and the compared point cloud using the point-to-mesh strategy.

[2] Print screens (PS) of Google Street View (GSV) from Google Maps (GM).

[3] Google Street View (GSV) images saved in Google Earth Pro (GEP).

[4] Comparison between the entire point clouds of May 2008 and June 2014 (Figure 3D).

[5] Comparison of a small cliff area of the May 2008 and June 2014 point clouds (Figure 3C).

[6] Comparison with the December 2016 LiDAR DEM (6'930'000 points) without vegetation from an assembly of six Optech terrestrial LiDAR clouds.

Using street view imagery for 3D survey of rock slope failures

J., Voumard[1], A., Abellan[1,2], P., Nicolet[1,3], M.-A. Chanut[4], M.-H., Derron[1], M., Jaboyedoff[1]

[1] Risk analysis group, Institute of Earth Sciences, FGSE, University of Lausanne, Switzerland
[2] Scott Polar Research Institute, Department of Geography, University of Cambridge, United Kingdom
[3] Geohazard and Earth Observation team, Geological Survey of Norway (NGU), Norway
[4] Groupe Risque Rocheux et Mouvements de Sols (RRMS), Cerema Centre-Est, France

Abstract

We discuss here different challenges and limitations on surveying rock slope failures using 3D reconstruction from image sets acquired from Street View Imagery (SVI). We show how rock slope surveying can be performed using two or more image sets using online imagery with photographs from the same site but acquired at different instants. Three sites in the French alps were selected as pilot study areas: (1) a cliff beside a road where a protective wall collapsed consisting of two images sets (60 and 50 images in each set) captured within a six years time-frame; (2) a large-scale active landslide located on a slope at 250 m from the road, using seven images sets (50 to 80 images per set) from 5 different time periods with three images sets for one period; (3) a cliff over a tunnel which has collapsed, using two image sets captured in a four years time-frame. The analysis include the use of different Structure for Motion (SfM) programs and the comparison between the so-extracted photogrammetric point clouds and a LiDAR derived mesh that was used as a ground truth. Results show that both landslide deformation and estimation of fallen volumes were clearly identified in the different point clouds. Results are site and software-dependent, as a function of the image set and number of images, with model accuracies ranging between 0.2 and 3.8 m in the best and worst scenario, respectively. Although some limitations derived from the generation of 3D models from SVI were observed, this approach allow obtaining preliminary 3D models of an area without on-field images, allowing extracting the pre-failure topography that would not be available otherwise.

Keywords

Street View Imagery (SVI), Structure from Motion (SfM), photogrammetry, 3D point cloud, natural hazard, landslide, rockfall.

1 Introduction

3D remote sensing techniques are becoming widely used for geohazard investigations due to their ability to represent the geometry of natural hazards (mass movements, lava flows, debris flows, etc.) and its evolution over time by comparing 3D point clouds acquired at different time steps. For example, 3D remote sensing techniques are helping to better quantify key aspects of rock slope evolution, including the accurate quantification of rockfall rates and the deformation of rock slopes before failure using both LiDAR (Rosser et al., 2005; Oppikofer et al, 2009; Royan et al., 2013; Kromer et al., 2015; Fey and Wichmann., 2016) and photogrammetrically derived point clouds (Walstra et al., 2007; Lucieer et al., 2013, Stumpf et al., 2015; Fernandes et al., 2016; Guerin et al., 2017; Ruggles et al., 2016).

Airborne and terrestrial laser scanner (ALS and TLS, respectively) are commonly used techniques to obtain 3D digital terrain models (Abellan et al., 2014). Despite their very high accuracy and resolution, these technologies are costly and often demanding from a logistic point of view. Alternatively, Structure from Motion (SfM) photogrammetry combined with multiview-stereo (MVS) allow using end-user digital cameras to generate 3D point clouds with a decimetre level accuracy in a cost-effective way in order (Westoby et al., 2012; Carrivick et al., 2016).

Whereas most of the studies in SfM literature utilise pictures that were captured on purpose (Eltner et al., 2016), the potential of using internet-retrieved pictures for 3D reconstruction has not been fully discussed before (e.g. Snavely et al., 2008; Guerin et al., 2017). One of the large sources of pictures on-line is the Street View Imagery (SVI) services, which offer 360 degrees panoramas from many roads, streets and other places around the world (Anguelov et al, 2013). It allows to remotely observe areas without physically accessing them and so in a cost-effective way, with applications in navigation, tourism, building texturing, image localization, point clouds georegistration and motion-from-structure-from-motion (Zamir et al. 2010; Anguelov et al, 2010; Klingner et al, 2013; Wang, 2013; Lichtenauer et al., 2015).

The aim of present work is to ascertain up to which extent 3D models derived from SVI can be used to detect geomorphic changes on rock slopes.

1.1 Street View Imagery

The most common SVI service is the well-known Google Street View (GSV) (Google Street View, 2017) that is available from Google Maps (Google Maps, 2017) or Google Earth Pro (Google Earth Pro, 2013). We used both GSV as SVI service in this study. Alternatives include StreetSide by Microsoft (StreetSide, 2017) and other national services like Tencent Maps in China (Tencent Maps, 2017). SVI was firstly deployed in urban areas to offer a virtual navigation into the streets. More recently, non-urban zones can also be accessed, and were used for the analysis of rock slope failures in this manuscript.

GSV was firstly used in May 2007 for capturing pictures in streets of the main cities in USA and it has been deployed worldwide over the forthcoming years, including also rural areas. GSV images are collected with a panoramic camera system mounted on different types of vehicles (e.g. a car, train, bike, snowmobile, etc.) or carried into a backpack (Anguelov et al, 2010).

The GSV first generation camera system was composed of eight wide-angle lenses and it is currently composed of fifteen CMOS sensors 5Mpx each (Anguelov et al, 2010). The fifteen raw images, which are not publicly available, are processed by Google to make a panorama view containing an a priori unknown image deformation (Figure 1). A GSV panorama is normally taken at an interval of around ten meters along a linear infrastructure (road, train or path).

GSV proposes a *back-in-time function* on a certain number of locations since April 2014. In addition, other historical GSV images are available from 2007 for selected areas only. The number of available image sets greatly varies at different locations: while some places have several sets, many other locations have only one image set. Back in time function is especially useful for natural hazards because it is possible to compare pre- and post-events images.

The GSV process can be explained in four steps (Anguelov et al, 2010; Google Street View, 2017): 1) Pictures acquisition in the field; 2) Image alignment: preliminary coordinates are given for each picture, extracted from sensors on the Google car that measure GNNS coordinates, speed and azimuth of the car, helping to precisely reconstruct the vehicle path. Pictures can also be tilted and realigned as needed; 3) Creation of 360° panoramas by stitching overlapping pictures. Google applies a series of processing algorithms to each picture to attenuate delimitations between each picture and to obtain smooth pictures transitions; 4) Panoramas draping on 3D models: the three LiDAR mounted on the Google car help to build 3D models of the scenes. 360° panoramas are draped on those 3D models to give a panorama view close to the reality. Each picture of the panorama has its own internal deformation, and the application of the processing chain described above makes inconstant deformation in the 360° panorama; in addition, the end-user does not have any information or control on it.

1.2 SfM-MVS

Structure for Motion (SfM) with Multi-View Stereo (MVS) dense reconstruction is a cost-effective photogrammetric method to obtain a 3D point cloud of terrain using a series of overlapping images (Luhmann et al., 2014). The prerequisites are that: (1) the studied object is photographed from different points of view, and (2) each element of the object must be captured from a minimum of two pictures assuming that the lens deformation parameters are known in advance (Snavely 2008; Lucieer et al. 2013). If these parameters are not known beforehand, three pictures is the minimum requirement (Westoby 2012), and about six pictures is preferred. The particularity of SfM-MVS is that prior knowledge of both intrinsic camera parameters (principal point, principal distance and lens distortion) and extrinsic camera parameters (orientation and position of the camera centre (Luhmann et al., 2014)) is not needed.

The workflow of SfM-MVS normally includes the following steps: 1) Feature detection and matching (Lowe, 1999); 2) Bundle adjustment (Snavely et al., 2006; Favalli et al., 2011; Turner et al., 2012; Lucieer et al., 2013); 3) Dense 3D point cloud generation (Furukawa et al., 2010; Furukawa & Ponce, 2010; James & Robson, 2012); and 4) Surface reconstruction and visualization (James & Robson, 2012).

2 Study areas and available data

We selected three study areas in France to generate point clouds from GSV images. This country was chosen because GSV cover the majority of the roads and because the timeline function works in most of the areas covered by GSV, meaning that several periods of acquisition are available. Moreover, landslide events occur regularly on French alpine roads. The aerial view of the three areas is shown in Figure 2A and examples of corresponding GSV images in Figure 2B and 2C.

The first case study (“Basse corniche” site) is a 20 m high cliff beside a main road in Roquebrune – Cap Martin connecting the town of Menton to the Principality of Monaco, in South-Eastern France. A wall built to consolidate the cliff collapsed after an extreme rainfall event in January 2014, blocking the road (Nice-Matin, 2014). Two 3D models were built with 60 GSV images taken in 2008 before the wall collapse, and 50 GSV images taken in 2014 after the event.

The second case studies is Séchilienne landslide, located 15 km South East of Grenoble (Isère department, France). The active area is threatening the departmental road RD 1091 connecting the towns of Grenoble and Briançon as well as a set of ski resorts such as L'Alpe d'Huez and Les Deux Alpes to the plain. This landslide is about 800 m long by 500 m high and it has been active during more than thirty years (Le Roux et al. 2009; Durville et al. 2011; Dubois et al. 2014). The shortest distance between the landslide foot and the former road was 250 m and the longest distance between the landslide head and the road is 1 km. A new road, located higher in the opposite slope, has been opened since July 2016. Different SfM-MVS processing were tested using from 50 up to 80 GSV images, at six different times from April 2010 to June 2015.

The third case study is located in "Arly gorges", between Ugine and Megève on the path Alberville – Chamonix-Mont-Blanc. A rockfall of about 8'000 m^3 affected the road at the entry of a tunnel on January 2014 (France 3, 2014). Different sets of images ranging from 60 to 110 GSV images were processed in order to obtain three 3D models of the road, the tunnel entry and the cliff above the tunnel.

We used two image sets from for the first study site, eight image sets for the second study site and four image sets for the third study site, with dates ranging from May 2008 up to December 2016, as described in Table 1.

3 Methodology

First step to make SfM-MVS with SVI is to obtain images from a SVI service. GSV has been used in this study (Figure 1). Given that original images of the Google cameras are not available, one of the two ways to get images from GSV is to manually extract them from the GSV panoramas. We took print screens (1920 x 1200 pixels, 2.3 Mpx) of GSV panoramas of the studied areas at each acquisition step, separated by about ten meters, from Google Maps. Several images were taken from the same point of view with different pan and tilt angles (Figure 1C) when the studied object was too close to the road. In such cases, it was impossible to have the entire area in one image because the image is not wide enough to capture the entire studied area (for example a 10 m high cliff along road). When the studied area was far away from the road, we took print screens of zoomed sections of the panorama.

To perform temporal comparisons on each site, images were taken at the different dates proposed by GSV with pre- and post-event images sets. We used the SfM-MVS program VisualSFM (Wu 2011) for dense point cloud reconstruction for the print screens images from Google Maps and we used CloudCompare (Girardeau-Montaut 2011) for point cloud visualization and comparison. Comparison between two point clouds was made using point-to-mesh strategy. To this end, a mesh was generated from the reference point cloud (the point cloud with the oldest images for site 1 or the LiDAR scans for sites 2 and 3) and then the other point cloud was compared to this reference mesh. The computed shortest distance, a signed value, between the mesh and the point cloud is the length of the 3D vector from the mesh triangle to the 3D point. Thus, average distances and standard deviations for each comparison of point clouds have been computed. Point density of point clouds was obtained using the "point density" function in CloudCompare with the "surface density" option.

Beside the images taken from print screens as described above, we also obtained GSV images (4800 x 3500 pixels, 16.8 Mpx) from Google Earth Pro on sites 2 and 3 with the "save image" function. This second way to get GSV allows to get images with a higher resolution than print screen images. Unfortunately, there is no timeline (or "back in time") function in Google Earth Pro; it is only possible to save images from the last picture acquisition, i.e. generally post-event images. GSV images from Google Earth Pro were processed with the Agisoft PhotoScan software (Agisoft 2015) for dense point cloud reconstruction, which provides much better results than VisualSFM. GSV images from Google Map were processed with VisualSFM because Agisoft was not able to process those print screens. The flowchart of Figure 3 shows the processing applied to both types of images (print screens and saved images).

A rough scaling and georeferencing of the 3D point clouds was made without ground control points, only with coordinates of few points extracted from Google Maps or from the French geoportal (Géoportail, 2016).

It is important to mention here that a series of issues are expected when attempting to use SVI for 3D model reconstruction with SfM-MVS. Indeed, GSV images are constructed as 360° panoramas from a series of pictures, so the internal deformation of the original image is not fully retained on the panoramas. In other words, the deformation of a cropped section of the panorama will be a main function not only of the internal deformation of the camera and lens but to the panorama reconstruction process; this circumstance will significantly influence the bundle adjustment process and so to the 3D reconstruction.

In addition, GoPro Hero4+ images from a moving vehicle on the road were taken by the authors on site 2, as well a series of images captured using a GoPro Hero5 Black camera standing on site 3 (image resolution of 4000 x 3000 pixels, 12 Mpx). Six LiDAR scans were also taken on site 3. This information was used for quality assessment purposes.

4 Results and discussion

Different results are obtained depending on the software used for SfM-MVS processing. For all case studies, VisualSFM gave results with print screens from GSV in Google Maps while Agisoft PhotoScan could not align those print screens despite adding a series of control points measured with Google Earth Pro. Resolution of print screens images seem to be insufficient to be processed with Agisoft PhotoScan. However, with higher point density and empty areas, Agisoft PhotosScan provided better results with images from Google Earth Pro than VisualSFM.

4.1 Site 1 – “Basse corniche” site

It was possible on “Basse Corniche” site to estimate the fallen volume by scaling and comparing the 2008 (Figure 4A) and 2010 (Figure 4B) point clouds. The 2008 point cloud is composed of 150’000 points with an average density of 290 points per square meter and the 2014 point cloud is composed of 182’000 points with an average density of 640 points per square meter (Table 1). VisualSFM could align the images and make 3D models before and after the wall collapse. It was possible to roughly scale and georeference the scene with the road width and few point coordinates measured on Google Earth Pro or on the French geoportal. After aligning the two 3D point clouds, meshes were built to compute the collapsed volume. The point-to-mesh alignment in CloudCompare of both point clouds was done on a small stable part of the cliff (Figure 4C) with a standard deviation of the point-to-mesh distance of about 10 cm (Figure 9 and Table 2) and on the entire cliff beside the vegetation with a standard deviation of about 25 cm (Figure 4E). In the collapsed area, the maximal horizontal distance between the two datasets is about 3.9 m (red colour in Figure 4D). The collapsed volume (including a possible empty space between the cliff and the wall before the event) was estimated to be about 225 m^3 using the point cloud comparison. Based on Google Street images, we manually estimated the dimensions of this volume (15 m long x 10 m high x 1.5 m deep), getting a similar value.

The obtained point clouds on site 1 allow to detect object of few decimetres. This accuracy was adequate to estimate the collapsed volume with an accuracy similar to the estimation made by hand based on the GSV photos and distances measured on Google Earth Pro and the French geoportal. This relatively high accuracy is due to the following factors: good image quality, reduced distance between the cliff and camera locations, good lighting conditions, absence of obstacles between the camera location and the area under investigation, no vegetation and efficient repartition of point of view around the cliff (Figure 2 A).

4.2 Site 2 – Séchilienne Landslide

Eight point clouds of which seven of SfM-MVS process with GSV images were generated for Séchillienne landslide at six different time steps (from April 2010 to June 2015). Three different image sources were used: GSV print screens from Google Maps, GSV images saved from Google Earth Pro and images from a GoPro HERO4+ camera from a moving vehicle (Figure 5 and Table 1). Two different programs (VisualSFM and Agisoft PhotoScan) were used for image treatment in function of the image sources (Figure 3 and Table 1). The number of 3D points on the landslide area varies from 9’500 to 22’500 points for a processing with VisualSFM with an average density of 0.25 to 0.85 points per square meter, while 236’000 3D points were generated when using Agisoft PhotoScan with an average density of 2 points per square meter (Table 1). In comparison, 1’500’000 points were obtained on the same area using terrestrial photogrammetry with a 24 Mpx reflex camera.

Results were aligned on a 50 cm resolution airborne LiDAR scan of the landslide acquired in 2010. Then, the street view SfM-MVS point clouds were aligned and compared with a mesh from the LiDAR scan using the point-to-mesh strategy. The alignment between the LiDAR point cloud and SfM-MVS point clouds derived from SVI is a key factor to define the quality of the clouds comparison. This alignment on stable areas (manually selected) was not easy to perform because of the low density of points on the SfM-MVS clouds derived from SVI. We noted a huge difference in the number of points between the different SfM-MVS clouds derived from SVI. This difference on the number of points shows the impacts of the image quality. Images with a good quality (resolution, exposition, sharpness) will give point clouds with a higher number of points as point clouds from low quality images.

Comparison results between SfM-MVS point clouds derived from SVI and airborne LiDAR scan highlight surface changes in the Séchilienne landslide over the years (Figure 8 and Table 1). The 2010 point cloud (Figure 5 A2) compared with 2010 LiDAR scan does not show any significant changes. Orange and red colours small dots are spread out on the entire landslide surface suggesting artefacts and not a real slope change. The 2010-2011 point clouds comparison (Figure 5 B2) shows few little red colour pattern (materiel accumulation) in the deposition and in the failure areas. The 2016 point cloud (Figure 5 C2) highlights material deposition in red colour, in the left part. This is confirmed with comparison of a 2013 terrestrial LiDAR. The blue colour pattern indicate a loss of material in the failure and the toe areas. The 2014 point cloud (Figure 5 D2) shows similar results than the 2013 point cloud with however a light increase of material in the deposition area and rock loss in the failure area. The 2010 to 2014 point clouds (Figure 5 A-D) were process with VisualSFM with GSV print screens in Google Maps (Table 1).

Three 2015 point clouds were processed: the first with VisualSFM and GSV print screens (Figure 5E), the second with VisualSFM with GSV images from Google Earth Pro (Figure 5F) and the third with Agisoft PhotoScan with images form Google Earth Pro again (Figure 5G). The results should be the same for the three point clouds but we noticed significant differences. The 2015 point cloud processed with VisualSFM and GSV images from Google Earth Pro (4800 x 3500 pixels), has a higher point density than the 2015 point cloud processed with GSV print screens (1920 x 1200 pixels). The 2015 point cloud with Agisoft PhotoScan and images from Google Earth Pro has a point density significantly higher (Table 1). The accumulation material (red colour in the left part) in the deposition area is clearly observable on the three 2015 point clouds, as the rock displacement-toppling below the failure area (red colour pattern in the failure area viewed as a material accumulation from the road). The loss of material (blue colour) is also well observable in the failure area and, to a lesser extent, in the right part of the deposition area. The last 2015 point cloud is very similar to the 2016 GoPro point cloud (Figure 5 H2) which confirms the results of SfM-MVS processing with GSV images.

Results of site 2 show that images with low resolution and with low lighting generated a lower number of points compared to the models generated with the last generation of GSV cameras, having higher resolution, more advanced sensors and pictures taken with favourable lighting conditions. The large distance between the road and the landslide considerably limits the final accuracy due to low image resolution, as discussed in Eltner et al., 2016; the closest distance between the road and the centre of the landslide is 500 m and the largest distance between the upper part of the landslide and the point of view is about 1’400 m. Furthermore, the vegetation on the landslide foot and along the road as well as a power line partially obstruct the visibility of the study area. In addition, clouds are present on several images on the top of the scarp, degrading the upper part of the 3D point cloud.

4.3 Site 3 – Arly Gorges

Four point clouds of which three of SfM-MVS process derived from GSV images were generated on the "Arly gorges" site, at four different times (from March 2010 to December 2016). Three different images sources (GSV print screens from Google Maps, GSV images exported from Google Earth Pro and our own images acquired from a GoPro HERO5 Black) were used (Figure 6 and Table 1). Two different programs (VisualSFM and Agisoft PhotoScan) were tested. In addition, a LiDAR point cloud resulting from an assembly of six Optech Ilris scans has been used as ground truth (Figure 6E). The number of points varies from 35'000 points to 3.2 million points with an average density of 40 to 2'200 points per square meter (Table 1).

The 3D point cloud from the "GoPro Hero5 Black" images has been roughly georeferenced, scaled and oriented thanks to the GNSS chip integrated in the camera and has been controlled and refined with points coordinates extracted from Google Maps and the French geoportal. The three point clouds processed from GSV images and the LiDAR scan have been roughly aligned to this reference. Then the four SfM-MVS point clouds (three with GSV images and one with GoPro images) were precisely aligned and scaled on the LiDAR point cloud, which was considered as the reference cloud.

The analysis (Figure 9, Tables 1 and 2) shows that the 2010 model derived from GSV images processed with VisualSFM gives the least accurate results (Figures 6A and 7A): we hardly perceive on that figure the wall of the tunnel entry and the wide cliff structures. The results of the 2014 point cloud from GSV images processed with the same program are slightly better (Figure 6B and 7B): the right-hand tunnel entry is modelled while it was not the case on the 2010 point cloud. The point cloud processed in Agisoft PhotoScan derived from 2016 GSV images saved from Google Earth Pro displays much better quality than the previous (Figure 6C and 7C): we now see the protective nets in the slope as well as the blue road sign announcing the tunnel. The vegetation is also observable and the tunnel entry is similarly modelled as the 2016 GoPro point cloud (Figure 6D).

The SfM-MVS point cloud derived from GoPro images gives a significantly better representation of the whole scene, especially on the top of the model. Slope structures and protective nets are well modelled, but not the small vegetation. The comparison between the

2016 LiDAR scan (Figure 6E) and the three SfM-MVS with GSV images point clouds does not allow to identify terrain deformation on the cliff. Moreover, the source area of the rockfall is not observable from the GSV images because it is located higher in the slope, outside of the images.

A great majority of points consistently displayed distances between the LiDAR scan mesh and the SfM-MVS point clouds ranging between +/- 2 m (Figure 7 A-C). Protective nets degrade the results because it generates badly modelled surfaces corresponding to the nets on some cliff sections (such as the red-blue section on the top-right of the July 2014 cloud (Figure 7A)). Considering the tunnel entry (Figure 7 D-F) the average distance point clouds - LiDAR mesh varies from -3 to -6 cm (depends mainly on the alignments of the clouds). Standard deviations vary from 22 cm for the 2010 point cloud to 11 cm for the 2016 point cloud. On a part of the wall above the tunnel (grey colour polygon on Figure 7 D-F), the average distance point cloud - LiDAR mesh varies from -3 cm to -18 cm with standard deviations of 3 cm for the 2010 point cloud, 4 cm for the 2014 point cloud et 6 cm for the 2016 point cloud (Figure 9 and Table 2). We observe again on this site that the improvement of the GSV camera resolution and image quality improve the processing. The information on the pictures source, date, point density and on the program used is given in Table 1.

A strong limiting factor on this site is the non-optimal camera locations. Indeed, the location of the cliff above a tunnel portal does not allow for a lateral movement between the camera positions with regard to the cliff. The maximal viewing angle (in blue colour on the Figure 2A) is about 35° compared to 170° for the site 1, and 115° for the site 2, that is 3 to 5 time smaller than for the other studied sites.

4.4 Discussion

With the experience acquired during the research, we can highlight the following recommendations to improve results of SfM-MVS with SVI images. (A) Firstly, the distance between the image point of view and the subject and the size of the subject are important because it influences the pixel size on the subject. In case study 1, the location of the cliff next to the road (< 1 m) allows to get images with a good resolution for the studied object. In case study 2, the area under investigation is too far from the road (500 – 1’400 m) and small structures cannot be seen in the landslide. (B) Secondly, the ability to look at the scene from different angles (Figure 2A) is a determining factor to obtain good results. The greater is this “view angle”, the better the results will be. Case study 1 with a view angle of almost 180° is optimal because the object is observable from half a circle. View angle of case study 2 (115°) is enough to get many different views of the subject from different angles. The view angle is too narrow to have enough different point of view of the cliff on case study 3 (35°). (C) Thirdly, results are influenced by the image quality and especially by their exposition, contrast and type of sensor, which has progressively been improved during the last years. Image quality varies considerably on different images sets. Case study 1 is again the best study case in term of image quality. Both image sets have optimal solar exposition and shadows are not strong. Case study 2 has sets with very different images quality. Some sets are well exposed, others not. Clouds are present on few image sets. For case study 3, we have a lot of over- and underexposed images on behalf of the situation of the site (incised valley with a southwest oriented slope with a lot of light or shadow). The problem of images quality concerns Google too because it has removed from Google Maps very underexposed GSV images taken in August 2014 on site 3 at the end of 2016.

According to our findings, small landslides and rockfalls (<0.5 m^3) can be detected when the slope or the cliff is close to the road (0-10 m), as it was shown on site 1. Conversely, large slope movements and collapses (>1’000 m^3) can be detected when the studied area is far away from the road (up to 0.5-1 km) like on site 2. On such sites, small changes (<1 m^3) can correspond to either real rockfalls or errors resulting from processing like on the toe of almost all point 3D clouds of Séchilienne landslide (Figure 5 A2-H2). The measured differences between the point clouds on stable areas show interesting results once the point clouds alignment is well done. Thus, we observed standard deviations of few decimetre on stable areas on site 1 (Figure 3D), between 0.5 and 1.1 m on site 2 and between 11 and 22 m on the tunnel entry on site 3. Standard deviations increase on site 2 when point clouds are compared on their entire surface (Figure 5 A2-H2, Table 1). This is attributable to the occurrence of slope movements generating material increase or decrease and thereby, increasing standard deviations of the distance between the two compared point clouds. It can also be due to a bad 3D point cloud alignment. Indeed, cloud alignment is not always easy on some point clouds because of low point density, because of voids in the point clouds (like in the landslide toe in Figure 5 F2) and because of the roughness of the terrain. In such difficult alignment cases, it was tried to align the point clouds on stable parts where point density was high.

Our study highlighted important differences on 3D model reconstruction using different software, consistently with previous works (Micheletti et al., 2015; Gomez-Gutierrez et al., 2015, Niederheiser et al., 2016). Agisoft PhotoScan performed better than VisualSFM when using both GSV images from Google Earth Pro (Figure 5F-G) and pictures acquired from a GoPro Hero camera (Figure 5H). Nevertheless, VisualSfM performed better than Agisoft PhotoScan on print screens captures from SVI. The only difference between these sources of information is the resolution: 2.3 Mpx for print screens from Google Maps, 16.8 Mpx for images saved from Google Earth Pro (and 12 Mpx for GoPro camera), stressing the importance of picture resolution on the quality of the 3D model.

The point density was evaluated according to the distance between the image point of view and the subject and the image types and processing software. The obtained results and the derived trends indicate that the use of GSV images from Google Earth Pro with VisualSFM increases by a factor two the point density compared to the processing of GSV print screens with VisualSFM. The processing of GSV images from Google Earth Pro with Agisoft PhotoScan increases by a factor ten the point density compared to the processing of GSV print screens with VisualSFM (trend strips in Figure 8). The expected point density of the 3D point clouds from GSV print screens processed in VisualSFM of a subject located few meters from the camera ("Basse-Corniche" dots on Figure 8) is about 300 points/m^2, about 50 points/m^2 for an area located at about 100 m ("Arly" dots on Figure 8) and about 0.5 point/m^2 for an area located at about 700 m ("Séchilienne" dots on Figure 8).

Despite the above mentioned prospects, some drawbacks were also observed. The main limitation found in this study is that SfM-MVS processing is designed to retrieve the internal orientation of standard cameras, whereas the images used in this research do not correspond to a standard camera due the construction of the panoramas. Indeed, the main problem comes from the different deformations on GSV print screens or images due to the panoramas construction. Same radial deformations, that are stronger than common camera lens, on each images, like on fisheyes images from GoPro cameras, can be processed without limitation with SfM software like Agisoft PhotoScan. In addition, images from GSV are often over- or underexposed (case study 3) and their resolution is low for distant subjects (cases study 2 and 3), making difficult to obtain results with few decimetric accuracy with these constraints. Making zoomed print screens from GSV images do not allow increasing the SfM-MVS process results (case study 2) due to a low images resolution. Finally, the spatial repartition of SVI is often problematic because there are not enough images along the track path and because the road path does not often allow obtaining an efficient strategy concerning the camera positions around the studied area (case study 3). Accessing to original (RAW) images together with valuable data of camera calibration would considerably help deriving 3D point clouds from GSV using modern photogrammetric workflows.

A simple development to improve our proposed approach would be that Google add the *back in time function* into the Google Earth Pro. In this case, it would be possible to save GSV images from any proposed time period and to process those images with Agisoft PhotoScan (Figure 5G) and thus to obtain better results than when using VisualSFM (Figure 5F). Knowing that Google services and functionalities of Google Maps and Google Earth are evolving over time, it is possible that SfM-MVS with GSV images will be more efficient and easier in a near future.

5 Conclusions

In this study it was possible to detect and characterize small landslides and rockfalls (<0.5 m^3) for study areas relatively close to the road (from 0 to 10 m); complementarily, it was possible to detect large scale landslides or rock collapses (>1’000 m^3) over areas located far away from the road (hundred meters or more). This information is of great interest when no other data of the studied area has been obtained.

The proposed methodology provides interesting but challenging results due to some constraints linked to the quality of the input imagery. The inconsistent image deformations and the impossibility of extracting the original images from a street view provider are the most important limitations for 3D model reconstruction derived from SVI. Following constraints strongly limit the proposed approach: large distances between the camera position and the subject of investigation, presence of obstacles between the studied area and the road, image quality, poor meteorological conditions, non-optimal images repartition, reduced number of images, existence of shadows/highlighted areas. The quality of the final product was observed to be mainly dependent on the images quality and of the distance between the studied area and image perspectives.

Although of the above mentioned limitations, SfM-MVS with SVI can be a useful tool in geosciences to detect and quantify slope movements and displacements at an early stage of the research by comparing datasets taken at different time series. The main interest of the proposed approach is the possibility to use archival imagery and deriving 3D point clouds of an area that has not been captured before the occurrence of a given event. This will allow increasing database on rock slope failures, especially for slope changes along roads which conditions are favourable for the proposed approach.

6 References

Abellán, A., Oppikofer, T., Jaboyedoff, M., Rosser, N.J., Lim, M. and Lato, M.J., 2014, Terrestrial laser scanning of rock slope instabilities. Earth Surface Processes and Landforms, v. 39, p.80-97.

Agisoft, L. L. C., 2015, Agisoft PhotoScan user manual, Professional edition, version 1.2.6.

Anguelov, D., Dulong, C., Filip, D., Frueh, Ch., Lafon, S., Lyon, R., Ogale, A., Vincent, L., Weaver, J., 2010, Google Street View: Capturing the world at street level. Computer, Vol. 43, IEEE, 32-38.

Carrivick, J. L., Smith, M. W., Quincey, D. J., 2016, Structure from Motion in the Geosciences. John Wiley & Sons.

Dubois, L., Chanut, M.-A., Duranthon, J.-P., 2014, Amélioration continue des dispositifs d'auscultation et de surveillance intégrés dans le suivi du versant instable des Ruines de Séchilienne. Géologues n°182, p50-55.

Durville, J.-L., Bonnard, C., Potherat, P., 2011, The Séchilienne (France) landslide: a non-typical progressive failure implying major risks, Journal of Mountain Science, Vol. 8, Issue 2, 117-123.

Eltner, A., Kaiser, A., Castillo, C., Rock, G., Neugirg, F. and Abellán, A., 2016, Image-based surface reconstruction in geomorphometry–merits, limits and developments. Earth Surface Dynamics, 4(2), pp.359-389.

Favalli, M., Fornaciai, A., Isola, I., Tarquini, S., Nannipieri, L., 2011, Multiview 3D reconstruction in geosciences, Computers & Sciences 44, 168-176.

Fey, C., Wichmann, V., 2016, Long-range terrestrial laser scanning for geomorphological change detection in alpine terrain – handling uncertainties. Earth Surf. Process. Landforms.

Fernández, T., Pérez, J. L., Cardenal, J., Gómez, J. M., Colomo, C., Delgado, J., 2016, Analysis of Landslide Evolution Affecting Olive Groves Using UAV and Photogrammetric Techniques. Remote Sensing, 8(10), 837.

Furukawa, Y., Ponce, J., 2010, Accurate, dense, and robust multiview stereopsis. Pattern Analysis and Machine Intelligence, IEEE Transactions on, 32(8), 1362-1376.

Furukawa, Y., Curless, B., Seitz, S. M., Szeliski, R., 2010, Towards internet-scale multi-view stereo. In Computer Vision and Pattern Recognition (CVPR), 2010 IEEE Conference on (pp. 1434-1441). IEEE.

France 3 : Important éboulement dans les gorges de l'Arly en Savoie, 2014, available at : http://france3-regions.francetvinfo.fr/alpes/savoie/important-eboulement-dans-les-gorges-de-l-arly-en-savoie-400849.html (last access 25 January 2017).

Géoportail, IGN (2016), 2016, available at http://www.geoportail.gouv.fr (last access 25 January 2017).

Girardeau-Montaut, D., 2011, CloudCompare-Open Source project. OpenSource Project.

Gómez-Gutiérrez, Á., de Sanjosé-Blasco, J.J., Lozano-Parra, J., Berenguer-Sempere, F. and de Matías-Bejarano, J., 2015, Does HDR pre-processing improve the accuracy of 3D models obtained by means of two conventional SfM-MVS software packages? The case of the Corral del Veleta Rock Glacier. Remote Sensing, 7(8), pp.10269-10294.

Google Street View, Understand Street View, 2017, available at https://www.google.com/maps/streetview/understand (last access 25 January 2017).

Google Maps, Google Inc. (2017), 2017, available at https://maps.google.com (last access 25 January 2017).

Google Earth Pro, version 7.1.2.241, Google Inc. (2013), 2013, available at https://www.earth.google.com/earth (last access 25 January 2017).

Guerin, A., Abellán, A., Matasci, B., Jaboyedoff, M., Derron, M.-H., and Ravanel, L.: Brief communication: 3-D reconstruction of a collapsed rock pillar from Web-retrieved images and terrestrial lidar data – the 2005 event of the west face of the Drus (Mont Blanc massif), Nat. Hazards Earth Syst. Sci., 17, 1207-1220, https://doi.org/10.5194/nhess-17-1207-2017, 2017.

James, M. R., Robson, S., 2012, Straightforward reconstruction of 3D surfaces and topography with a camera, Accuracy and geosciences application, Journal of Geophysical research, Vol. 117, F03017.

Klingner, B., Martin, D., Roseborough, J., 2013, Street View Motion-from-Structure-from-Motion, Proceedings of the International Conference on Computer Vision, IEEE.

Kromer, R., Abellán, A., Hutchinson, J., Lato, M., Edwards, T., Jaboyedoff, M., 2015, A 4D Filtering and Calibration Technique for Small-Scale Point Cloud Change Detection with a Terrestrial Laser Scanner. Remote Sensing vol.7, pp.13029-13052; DOI: 10.3390/rs71013029.

Lichtenauer, J. F., Sirmacekb, B., 2015, A semi-automatic procedure for texturing of laser scanning point with google streetview images, The International Archives of the Photogrammetry, Remote Sensing and Spatial Information Sciences, Volume XL-3/W3, 109-114.

Le Roux, O., Schwartz, S., Gamond, J. F., Jongmans, D., Bourles, D., Braucher, R., Mahaney, W., Carcaillet, J., Leanni, L., 2009, CRE dating on the head scarp of a major landslide (Séchilienne, French Alps), age constraints on Holocene kinematics, Earth and Planetary Science Letters, Vol. 280, 236-245.

Lucieer, A., de Jong, S., Turner, D., 2013, Mapping landslide displacements using Structure from Motion (SfM) and image correlation of multi-temporal UAV photography, Progress in Physical Geography, Vol. 38(1), 97-116.

Luhmann, T., Robson, S., Kyle, S., Boehm, J., 2014, Close-range photogrammetry and 3D imaging. Walter de Gruyter.

Lowe, D., 1999, Object recognition from local scale-invariant features. International Conference of Computer Vision, Corfu Greece, 1150-1157.

Luhmann, T., Robson, S., Kyle, S., Boehm, J., 2014, Close-range photogrammetry and 3D imaging, Walter De Gruyter.

Micheletti, N., Chandler, J. H., Lane, S. N., 2015, Investigating the geomorphological potential of freely available and accessible Structure-from-Motion photogrammetry using a smartphone. Earth Surface Processes and Landforms, Vol 40(4), 473-486.

Nice-Matin : La basse corniche coupée en direction de Monaco après un éboulement, 2014, available at : http://www.nicematin.com/menton/la-basse-corniche-coupee-en-direction-de-monaco-apres-un-eboulement.1587292.html (last access 15 October 2015).

Niederheiser, R., Mokroš, M., Lange, J., Petschko, H., Prasicek, G., & Elberink, S. O., 2016, Deriving 3d Point Clouds from Terrestrial Photographs-Comparison of Different Sensors and Software. International Archives of the Photogrammetry, Remote Sensing and Spatial Information Sciences-ISPRS Archives, 41, 685-692.

Oppikofer, T., Jaboyedoff, M., Blikra, L., Derron, M.-H., Metzger, R., 2009, Characterization and monitoring of the Åknes rockslide using terrestrial laser scanning. Natural Hazards and Earth System Science 9: 1003–1019.

Rosser, N.J., Petley, D.N., Lim, M., Dunning, S.A., Allison, R.J., 2005, Terrestrial laser scanning for monitoring the process of hard rock coastal cliff erosion. Quarterly Journal of Engineering Geology and Hydrogeology 38(4): 363–375.

Royán, M.J., Abellán, A., Jaboyedoff, M., Vilaplana, J. M., Calvet, J.,2014, Spatio-temporal analysis of rockfall pre-failure deformation using Terrestrial LiDAR. Landslides, pp.1–13.

Ruggles, S., Clark, J., Franke, K. W., Wolfe, D., Reimschiissel, B., Martin, R. A., ... & Hedengren, J. D.,2016, Comparison of SfM computer vision point clouds of a landslide derived from multiple small UAV platforms and sensors to a TLS-based model. Journal of Unmanned Vehicle Systems, 4(4), 246-265.

Snavely, N., M. Seitz, S., Szeliski, R., 2006, Photo Tourism: Exploring Photo Collection in 3D. In SIGGRAPH 06, 835-846.

Snavely, N., 2008, Scene reconstruction and visualization from Internet photo collections, unpublished PhD thesis, University of Washington, USA.

Snavely, N., Seitz, S., Szeliski, R., 2008, Modeling the World from Internet Photo Collections Int J Comput Vision, Springer Netherlands, 80, 189-210

Streetside, Microsoft Inc. (2017), 2017, available at https://www.microsoft.com/maps/streetside.aspx (last access 25 January 2017).

Stumpf, A., Malet, J. P., Allemand, P., Pierrot-Deseilligny, M., Skupinski, G., 2015, Ground-based multi-view photogrammetry for the monitoring of landslide deformation and erosion. Geomorphology, 231, 130-145.

Tencent Maps, Tencent Inc. (2017), 2017, available at http://map.qq.com (last access 25 January 2017).

Turner, D., Lucieer, A., Watson, C., 2012, An Automated Technique for Generating Georectified Mosaics, from Ultra-High Resolution Unmanned Aerial Vehicle (UAV), Conference on 3D Imaging, Modeling, Processing, Visualization & Transmission Imagery, Based on Structure from Motion (SfM) Point Clouds, Remote Sensing, 4(5), 1392-1410 IEEE,479-486.

Walstra, J., Chandler, J. H., Dixon, N., Dijkstra, T. A., 2007, Aerial photography and digital photogrammetry for landslide monitoring. Geological Society, London, Special Publications, 283(1), 53-63.

Wang, C.-P., Wilson, K., Snavely, N., 2013, Accurate Georegistration of Point Clouds Using Geographic Data, In 3D Vision – 3DV, IEEE, 33-40.

Westoby, M.J., Brassington, J., Glasser, N.F., Hambrey, M.J., Reynolds, J.M., 2012, ‘Structure-from-Motion’ photogrammetry: A low-cost, effective tool for geoscience applications, Geomorphology, Vol. 179, 300-314.

Wu, C., 2011, VisualSFM: A visual structure from motion system, available at http://ccwu.me/vsfm (last access 25 January 2017).

Zamir, A. R., Shah, M., 2010, Accurate Image Localization Based on Google Maps Street View, In Computer Vision – ECCV 2010, Springer, 255-268.

7 Figures

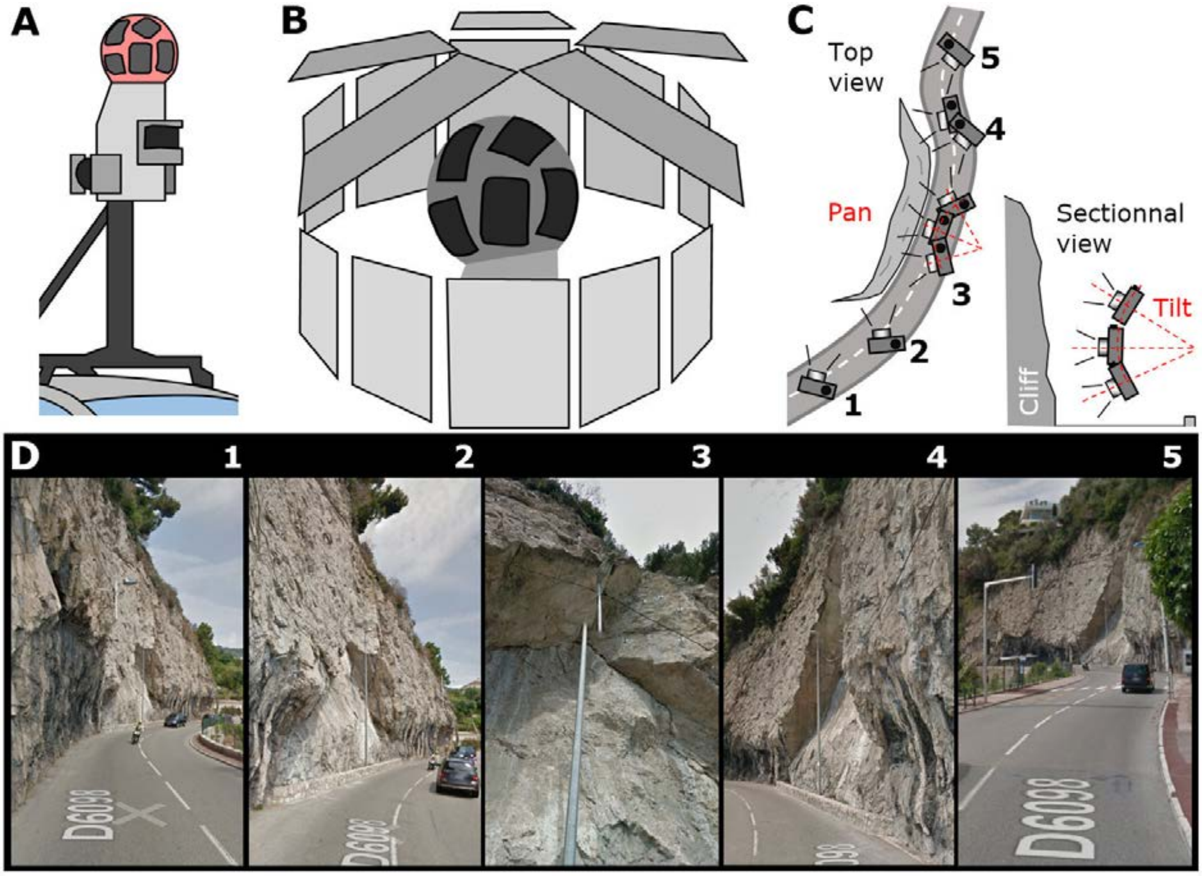

Figure 1: Google Street View (GSV) imagery functioning. A: Schema of the GSV spherical camera system mounted on a car roof. Sensors in black colour are LiDAR on which are draped the GSV images (based on Google Street View 2017). B: Functioning of the GSV spherical panorama built with fifteen images. C: Strategy of the GSV service for SfM-MVS photogrammetry. Numbers correspond schematically to the images in D. D: Screen captures of GSV photos from the study site 1. The image numbers correspond to those in C. Note the gap on the street-lamp in images 3 due to the panorama construction from the GSV pictures.

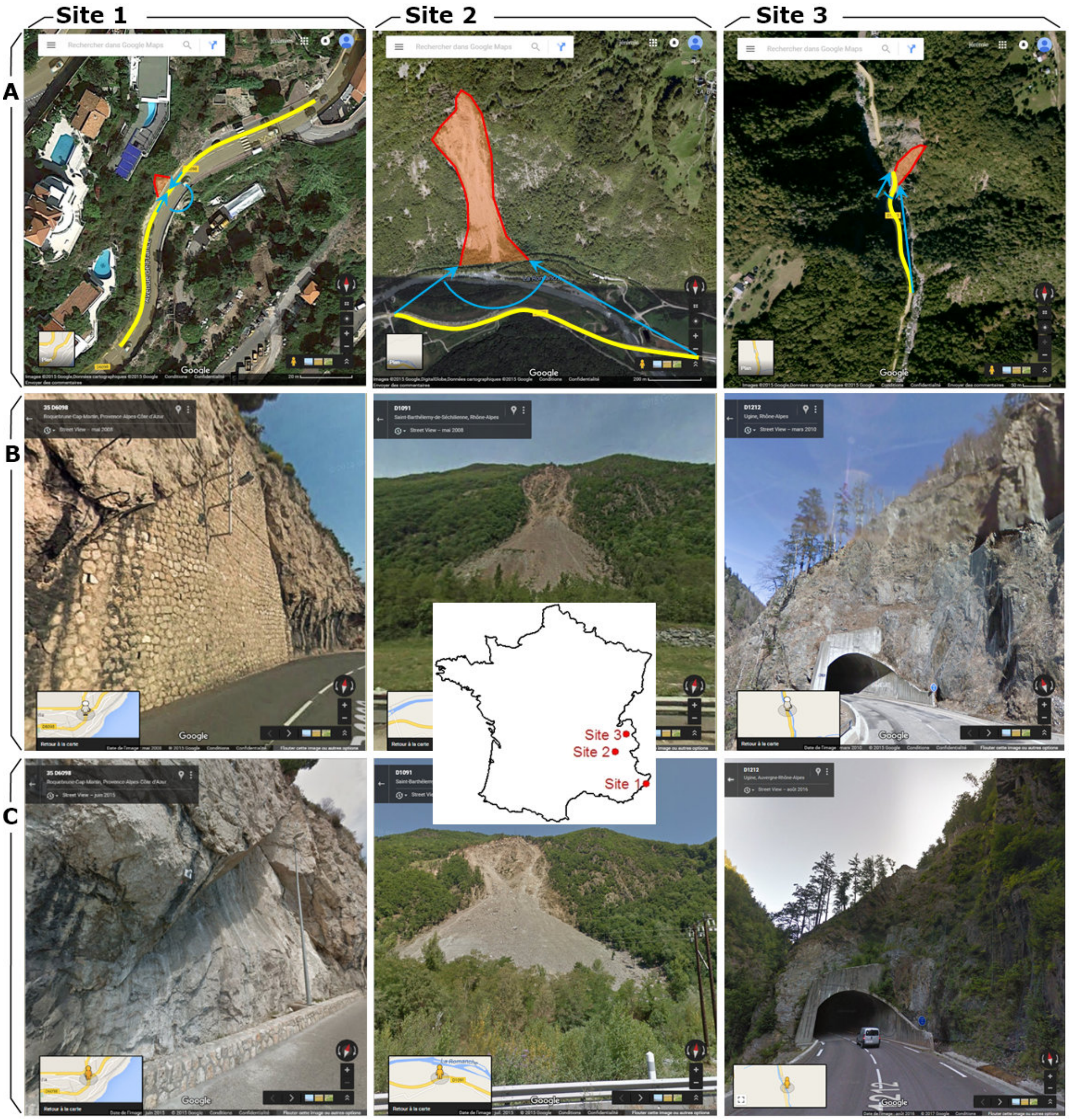

Figure 2 : The three French studied sites (1: Basse-Corniche, 2: Séchilienne and 3: Arly gorges). A: Google Maps aerial view of the sites (in red) with the road path (yellow) used to take the GSV images of the scenes and the view angle (blue) of the images point of view around the sites. B: First GSV of the sites. C: Last GSV of the sites.

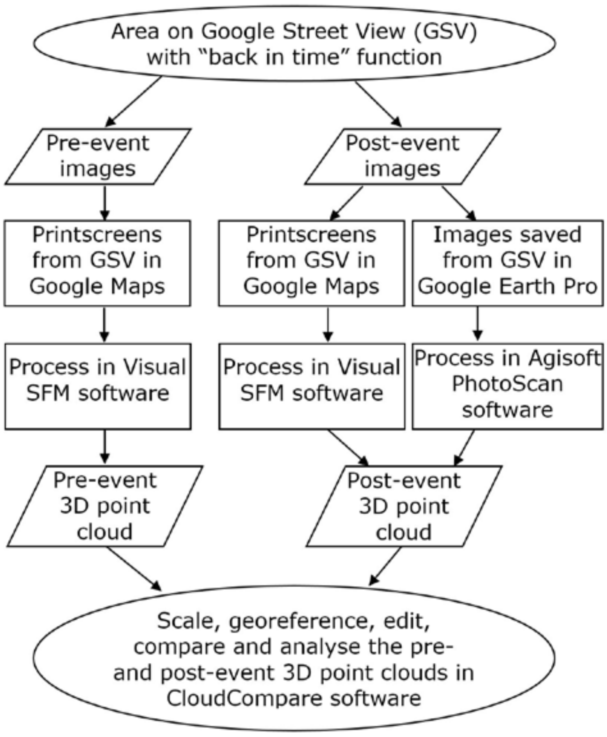

Figure 3: Flowchart of the SfM-MVS processing with GSV images on an area with the "back in time" function available. Pre-event images are displayed using the "back in time" function in GSV. Post-event images arise either from print screens of GSV in Google Maps using or not the "back in time" function or from GSV images saved in Google Earth Pro. In this last case, the last available proposed GSV images have a greater resolution as the print screens and can be processed in the Agisoft PhotoScan.

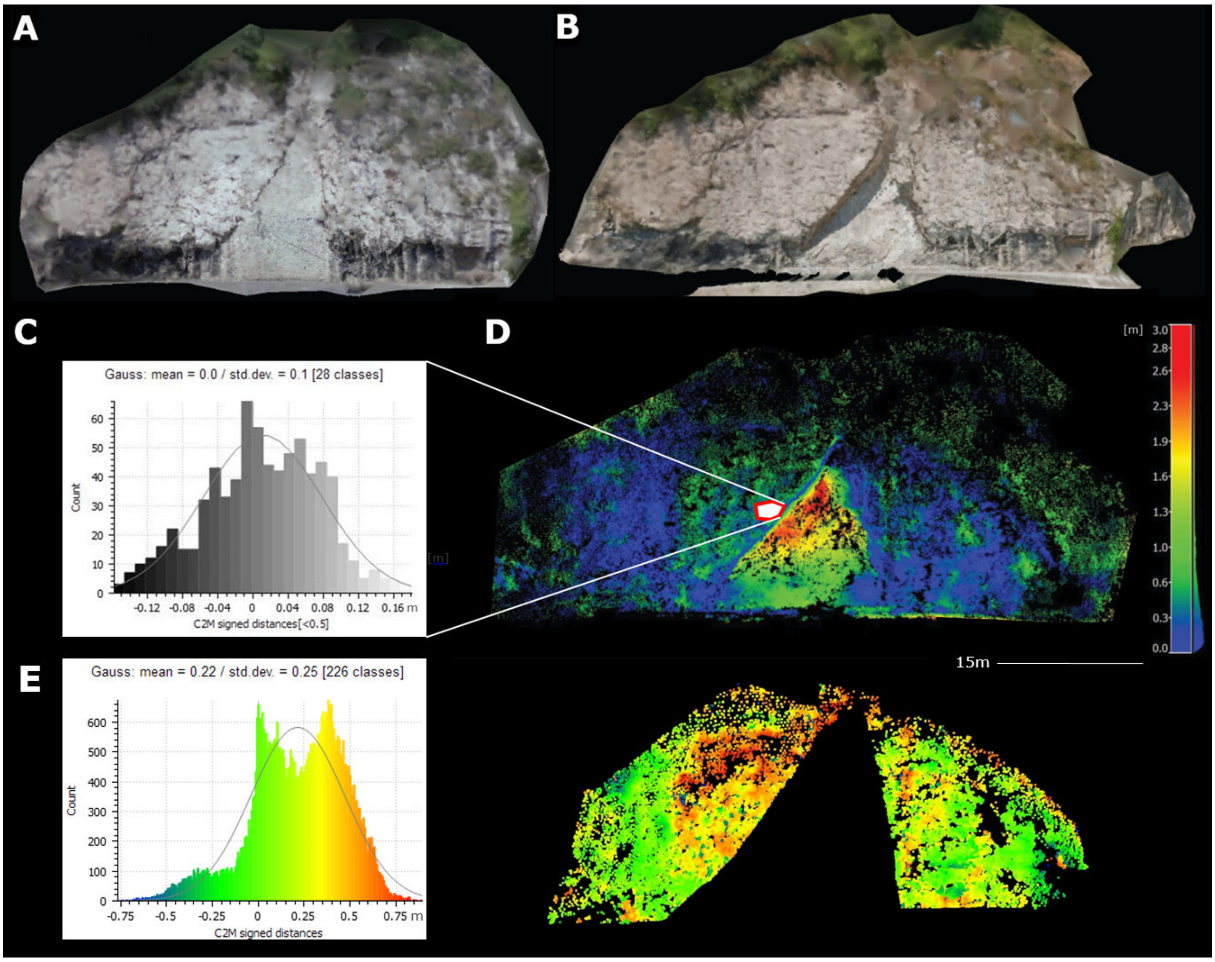

Figure 4: Results at site 1 "Basse-Corniche". A: 3D model produced with GSV images taken before the event in 2008. B: 3D model produced with GSV images taken after the event in 2014. C: Statistics on a small part of the wall (red colour polygon on figure D) of 7'510 points between the two point clouds with the point-to-mesh strategy in the CloudCompare. D: Comparison of the two point clouds of 2008 and 2014 on the entire surface of the 3D point clouds. The maximal horizontal depth of the cliff is about 3.9 m. E: Comparison of the two point clouds of 2008 and 2014 on the entire stable parts of the cliff (i.e. without vegetation) by not taking into account the collapsed wall (black triangle in the centre of the point clouds. The information on the pictures source, date, point density and on the program used is given in Tables 1 and 2.

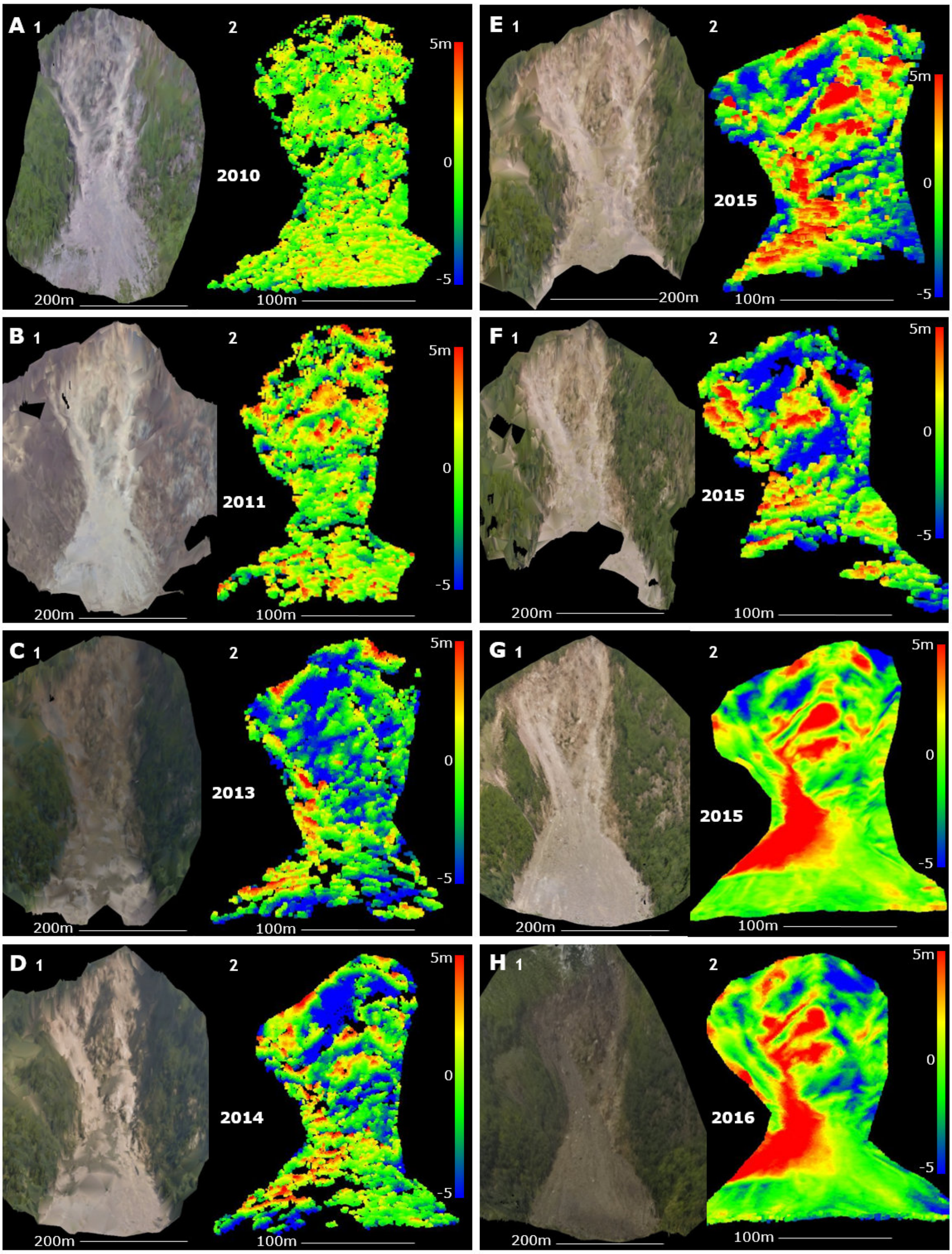

Figure 5 : Results at site 2 "Séchilienne". Eight points clouds from different images sets taken at six different time with three different image sources and processed with two different programs. Figures A1-H1: Meshs resulting from the respective point clouds. Figures A2-H2: point clouds comparison with a 50 cm LiDAR DEM from 2010 (red colour points is material increase; blue colour points are material decrease from the 2010 LiDAR cloud) with the point-to-mesh strategy in CloudCompare. The information on the pictures source, date, point density and on the program used is given in Table 1.

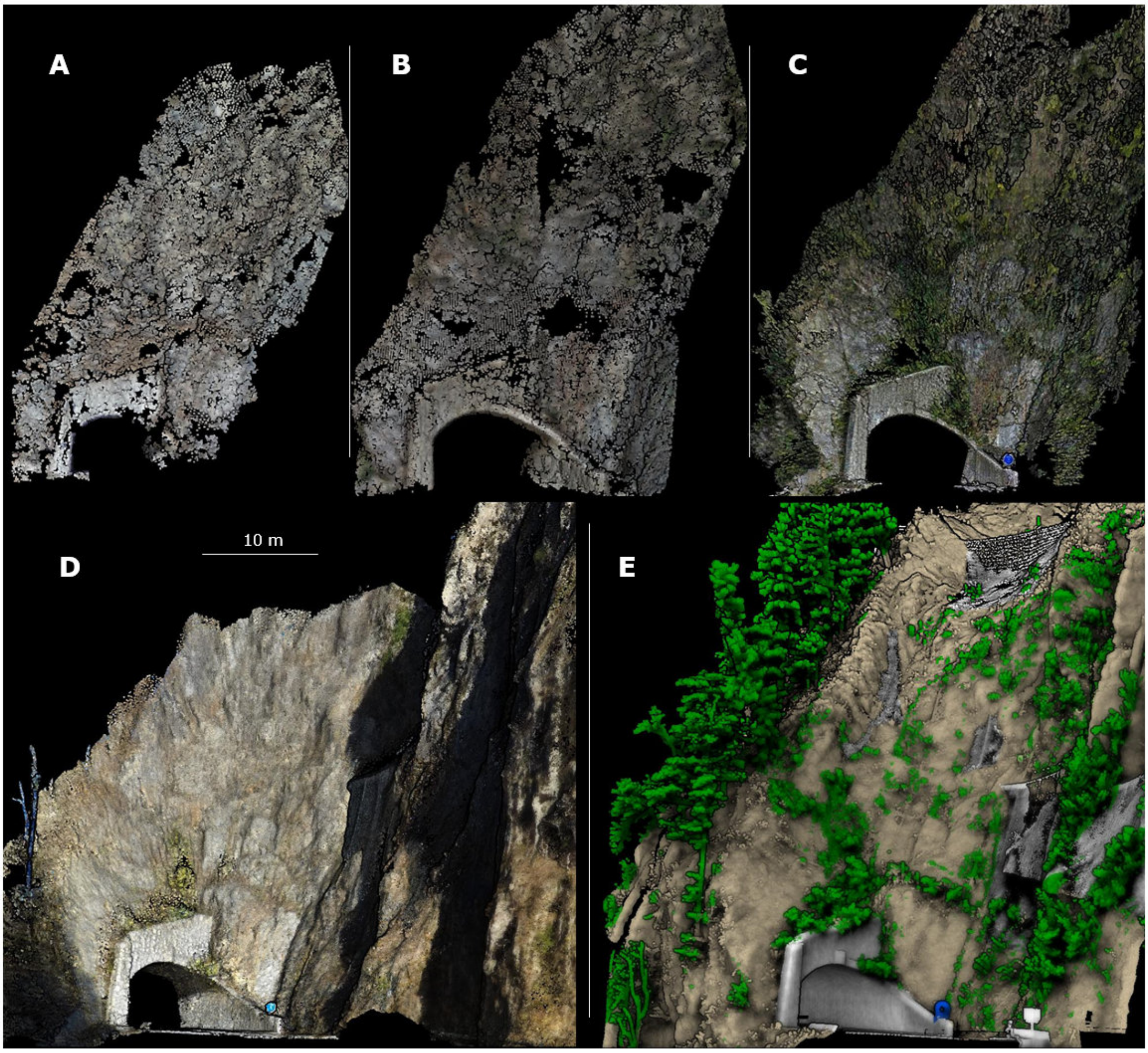

Figure 6 : Results at site 3 "Arly gorges". Five points clouds from four different images sets sources and processed with two different softwares and one LiDAR scan. A: March 2010 point cloud. B: July 2014 point cloud. C: August 2016 point cloud. D: December 2016 point cloud taken on foot with a GoPro camera. E: December 2016 LiDAR cloud from an assembly of six Optech terrestrial LiDAR scans. The grey elements in the cliff are the protective nets.

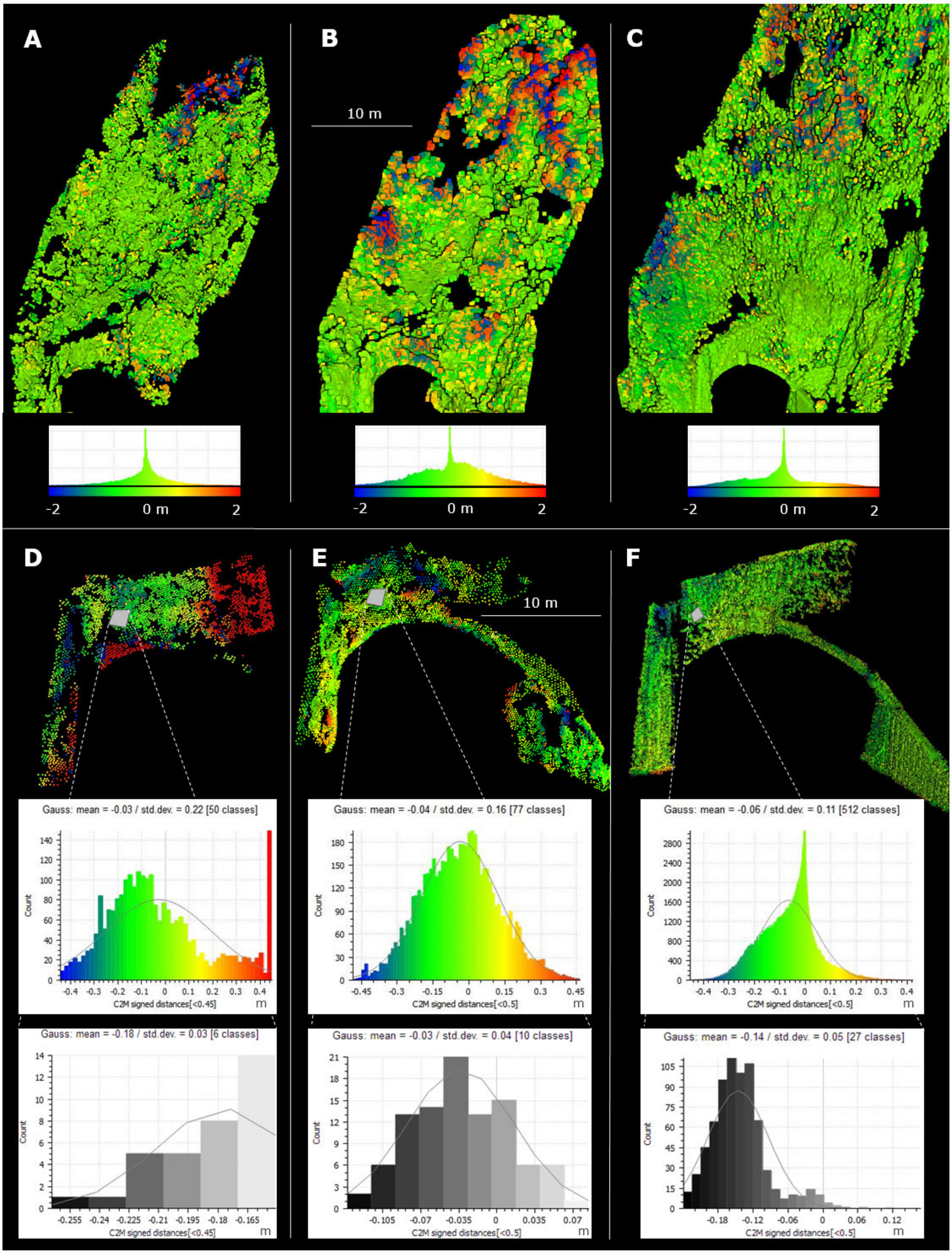

Figure 7: A-B-C: March 2010, July 2014 and August 2016 point clouds compared with December 2016 LiDAR DEM (red colour points is material increase; blue colour points are material decrease from the 2016 LiDAR cloud) with the point-to-mesh strategy on the CloudCompare. D, E, F: tunnel entry and part of the wall overlooking the tunnel (grey colour polygon) of the March 2010, July 2014 and August 2016 point clouds compared with December 2016 LiDAR DEM. The information on the pictures source, date, point density and on the program used is given in Tables 1 and 2.

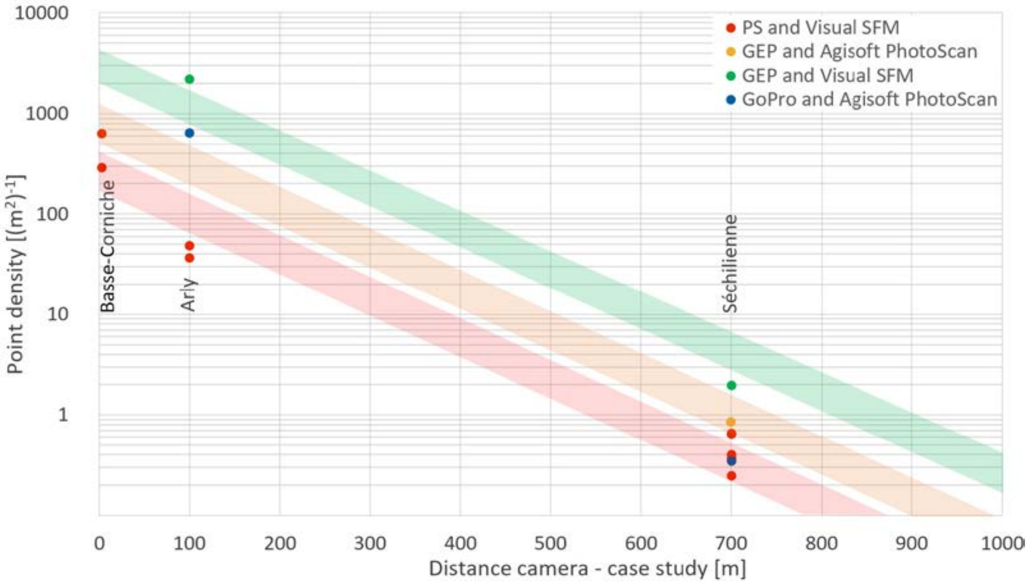

Figure 8: Correlation between distance camera - case studies and the expected density of points from the three case studies. The red colour dots are results of the three case studies point clouds obtained from Google Street View (GSV) print screens (PS) in Google Maps (GM) processed with VisualSFM. The red strip represents the corresponding trend based on a negative exponential function. The orange colour dot is the result of the Séchilienne point cloud obtained from GSV images saved in Google Earth Pro (GEP) processed with VisualSFM. The orange strip represents the corresponding trend based on a negative exponential function. The green colour dots are results of the Séchilienne and Arly point clouds obtained from GSV images saved in (GEP) processed with Agisoft PhotoScan. The green strip represents the corresponding trend based on a negative exponential function. By way of comparison, the blue colour dots represent the result of the Séchilienne and Arly point clouds obtained with GoPro action camera images taken on the field and processed with Agisoft PhotoScan.

Figure 9: Correlation between distance camera - case studies and the expected standard deviation from the three case studies. The dots are results of point clouds comparisons on the entire point cloud areas (Table 1). The triangle are results of point clouds comparisons on partial point cloud area (Table 2). The red colour dots and triangle are results of the three case studies point clouds obtained from Google Street View (GSV) print screens (PS) in Google Maps (GM) processed with VisualSFM compared on the entire area. The orange colour dot is the result of the Séchilienne point cloud obtained from GSV images saved in Google Earth Pro (GEP) processed with VisualSFM. The green colour dots and triangles are results of the Séchilienne and Arly point clouds obtained from GSV images saved in (GEP) processed with Agisoft PhotoScan. By way of comparison, the blue colour dots represent the result of the Séchilienne and Arly point clouds obtained with GoPro action camera images taken on the field and processed with Agisoft PhotoScan.

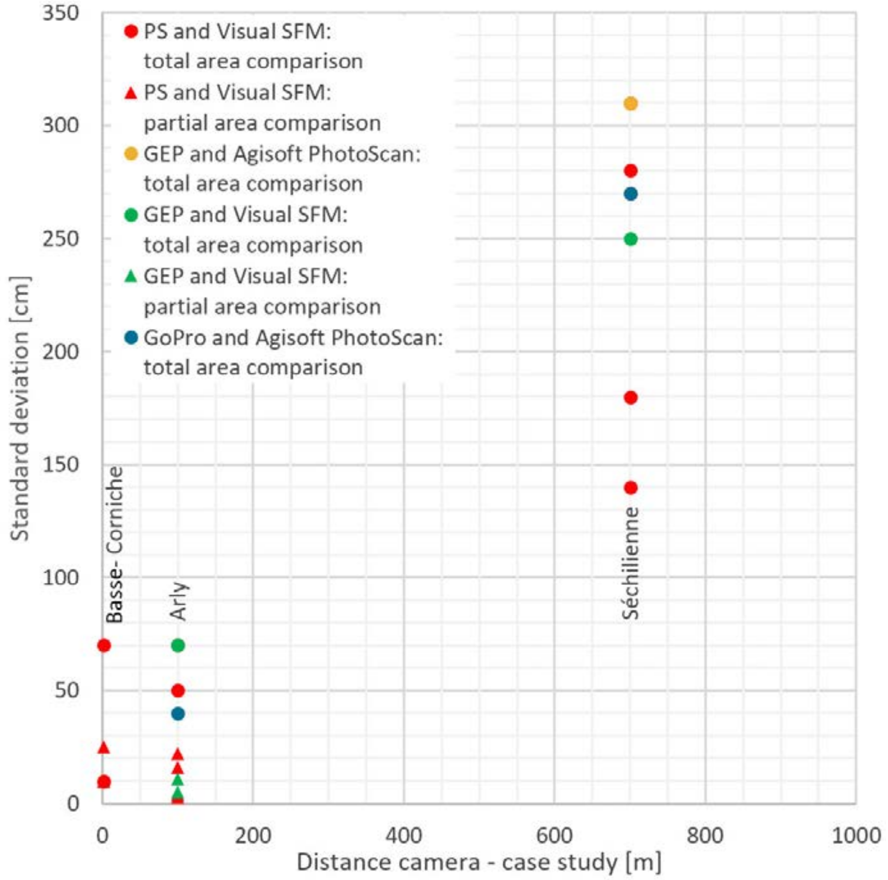

Table 1: List of the fourteen point clouds presented in this paper.

Site	Figure	Date	Images source	Images size [pixel]	Images number	Point density[1] (pts/m²)	Processing software	Number of points	Comparison		
									With	Mean distance[2] [m]	Std. dev. [m]
Site 1	Fig. 4A	2008.05	PS GSV from GM[3]	1920 x 1200	60	290	VisualSFM	150’000	)14.06[7]	0.2	0.7
	Fig. 4B	2014.06	PS GSV from GM[3]	1920 x 1200	50	640	VisualSFM	182’000	)8.05[8]	0.0	0.1
Site 2	Fig. 5A	2010.04	PS GSV from GM[3]	1920 x 1200	54	0.40	VisualSFM	18’000	)AR[9]	-0.2	1.4
	Fig. 5B	2011.03	PS GSV from GM[3]	1920 x 1200	52	0.25	VisualSFM	9’500	)AR[9]	-0.1	1.8
	Fig. 5C	2013.05	PS GSV from GM[3]	1920 x 1200	45	0.37	VisualSFM	12’500	)AR[9]	-2.1	2.7
	Fig. 5D	2014.06	PS GSV from GM[3]	1920 x 1200	52	0.66	VisualSFM	25’000	)AR[9]	-1.5	2.8
	Fig. 5E	2015.06	PS GSV from GM[3]	1920 x 1200	62	0.64	VisualSFM	23’500	)AR[9]	-0.9	3.1
	Fig. 5F	2015.06	GSV from GEP[4]	4800 x 3500	80	0.86	VisualSFM	22’500	)AR[9]	-1.7	3.1
	Fig. 5G	2015.06	GSV from GEP[3]	4800 x 3500	80	1.99	Agisoft PhotoScan	236’000	)AR[9]	0.6	2.5
	Fig. 5H	2016.05	GoPro[5]	4000 x 3000	75	0.35	Agisoft PhotoScan	46’000	)AR[9]	-0.2	2.7
Site 3	Figs. 6A, 7A	2010.03	PS GSV from GM[3]	1920 x 1200	66	40	VisualSFM	35’000	)AR[10]	0.0	0.5
	Figs. 6B, 7B	2014.07	PS GSV from GM[3]	1920 x 1200	111	50	VisualSFM	53’000	)AR[10]	0.1	0.7
	Figs. 6C, 7C	2016.08	GSV from GEP[2]	4800 x 3107	64	2200	Agisoft PhotoScan	3’1850’000	)AR[10]	-0.1	0.7
	Fig. 6D	2016.12	GoPro[6]	4000 x 3000	50	650	Agisoft PhotoScan	2’217’000	)AR[10]	0	0.4

[1] Point density around a search radius of 2 m.
[2] Average distance between the mesh of the reference point cloud and the compared point cloud using the point-to-mesh strategy.
[3] Print screens (PS) of Google Street View (GSV) from Google Maps (GM).
[4] Google Street View (GSV) images saved in Google Earth Pro (GEP).
[5] GoPro Hero4+.
[6] GoPro Hero5 Black with GNSS chip integrated.
[7] Comparison between the entire point clouds of May 2008 and June 2014 (Figure 3D).
[8] Comparison of a small cliff area of the May 2008 and June 2014 point clouds (Figure 3C).
[9] Comparison with the 50 cm airborne LiDAR DEM from 2010.
[10] Comparison with the December 2016 LiDAR DEM (6’930’000 points) without vegetation from an assembly of six Optech terrestrial LiDAR clouds.

Table 2: List of the eight partial point cloud comparisons.

Site	Figure	Date	Images source	Images size [pixel]	Processing software	Comparison			
						Comparative area	With	Mean distance[1] [cm]	Std. dev. [cm]
Site 1	Fig. 4C	2008.05	PS GSV from GM[2]	1920 x 1200	VisualSFM	Small cliff part	4.06[4]	0	10
	Fig. 4E	2008.05	PS GSV from GM[2]	1920 x 1200	VisualSFM	Entire cliff without wall and vegetation	4.06[4]	22	25
Site 3	Fig. 7D 1	2010.03	PS GSV from GM[2]	1920 x 1200	VisualSFM	Tunnel entry	)AR[5]	-3	22
	Fig. 7D 2	2010.03	PS GSV from GM[2]	1920 x 1200	VisualSFM	Small part of tunnel entry	)AR[5]	-18	3
	Fig. 7E 1	2014.07	PS GSV from GM[2]	1920 x 1200	VisualSFM	Tunnel entry	)AR[5]	-4	16
	Fig. 7E 2	2014.07	PS GSV from GM[2]	1920 x 1200	VisualSFM	Small part of tunnel entry	)AR[5]	-3	4
	Fig. 7F 1	2016.08	GSV from GEP[3]	4800 x 3107	Agisoft PhotoScan	Tunnel entry	)AR[5]	-6	11
	Fig. 7F 2	2016.08	GSV from GEP[3]	4800 x 3107	Agisoft PhotoScan	Small part of tunnel entry	)AR[5]	-14	5

[1] Average distance between the mesh of the reference point cloud and the compared point cloud using the point-to-mesh strategy.
[2] Print screens (PS) of Google Street View (GSV) from Google Maps (GM).
[3] Google Street View (GSV) images saved in Google Earth Pro (GEP).
[4] Comparison between the entire point clouds of May 2008 and June 2014 (Figure 3D).
[5] Comparison of a small cliff area of the May 2008 and June 2014 point clouds (Figure 3C).
[6] Comparison with the December 2016 LiDAR DEM (6'930'000 points) without vegetation from an assembly of six Optech terrestrial LiDAR clouds.